LBL-20553
UC-11

Lawrence Berkeley Laboratory
UNIVERSITY OF CALIFORNIA

EARTH SCIENCES DIVISION

RECEIVED
LAWRENCE
BERKELEY LABORATORY

APR 25 1986

LIBRARY AND
DOCUMENTS SECTION

PRELIMINARY NUMERICAL SIMULATIONS OF GROUNDWATER FLOW IN THE UNSATURATED ZONE, YUCCA MOUNTAIN, NEVADA

J. Rulon, G.S. Bodvarsson, and P. Montazer

March 1986

For Reference

Not to be taken from this room

Prepared for the U.S. Department of Energy under Contract DE-AC03-76SF00098

LBL-20553 c.1

DISCLAIMER

This document was prepared as an account of work sponsored by the United States Government. While this document is believed to contain correct information, neither the United States Government nor any agency thereof, nor the Regents of the University of California, nor any of their employees, makes any warranty, express or implied, or assumes any legal responsibility for the accuracy, completeness, or usefulness of any information, apparatus, product, or process disclosed, or represents that its use would not infringe privately owned rights. Reference herein to any specific commercial product, process, or service by its trade name, trademark, manufacturer, or otherwise, does not necessarily constitute or imply its endorsement, recommendation, or favoring by the United States Government or any agency thereof, or the Regents of the University of California. The views and opinions of authors expressed herein do not necessarily state or reflect those of the United States Government or any agency thereof or the Regents of the University of California.

Preliminary Numerical Simulations of Groundwater Flow in the Unsaturated Zone, Yucca Mountain, Nevada

Jennifer Rulon and Gudmundur S. Bodvarsson

Earth Sciences Division
Lawrence Berkeley Laboratory
University of California
Berkeley, California 94720

Parviz Montazer

U.S. Geological Survey
Denver Federal Center
Denver, Colorado 80225

ABSTRACT

Numerical simulations of the natural state of the unsaturated zone underlying Yucca Mountain, Nevada, were performed. The hydrogeology at Yucca Mountain is characterized by fluid flow through heterogeneous, anisotropic, fractured tuff in an arid environment. The purpose of the study is to examine the general groundwater-flow patterns computed on the basis of the available data and to examine ideas contained in a proposed conceptual hydrologic model of the site. The model simulates two-dimensional liquid-water flow in a vertical cross section extending from the ground surface to the water table at a depth of about 650 m. Various fluxes representing the net infiltration were specified at the surface and the steady-state flux, liquid-saturation distribution, and matric-potential distribution were computed. The results indicate that because of the dip of the stratigraphic units and because of their hydraulic properties, a significant proportion of the flow above and/or below the proposed repository horizon is diverted laterally into a permeable fault zone. The magnitude and location of the lateral flow depend upon whether matrix-flow or fracture-flow conditions are assumed for the highly fractured units, upon the flux specified at the ground surface, and upon the hydraulic properties assigned to the fault zone. Various cases were considered to examine the liquid-water flux through the proposed repository unit; all of the results are controlled by poorly known hydraulic parameters such as the characteristic curves.

Table of Contents

List of Tables vi
List of Figures vii
Acknowledgements x
1.0 Introduction 1
2.0 Available Data 5
2.1 General Hydrogeologic Setting 5
2.2 Hydraulic Properties of the Units 7
2.2.1 Matrix Characteristic Curves 10
2.2.2 Fracture Characteristic Curves 16
2.3 Natural-State Data 18
2.3.1 Precipitation Data 18
2.3.2 Profiles of Water Potential and Liquid Saturation 18
3.0 Conceptual Model 23
4.0 Numerical Model 27
5.0 Theoretical Studies 28
5.1 One-Dimensional Flow Simulations 28
5.2 Two-Dimensional Flow Simulations 36
5.2.1 Matrix-Flow Simulations 38
5.2.2 Fracture-Flow Simulations 46
5.2.3 Fracture-Matrix Flow Simulations 50
5.2.4 Sensitivity Studies 58
Fault-Zone Properties 62
Second Fault Zone 65
Mesh Dependence 68
6.0 Discussion 71
6.1 Comparison with Field Data 71
6.1.1 Matric Potential 74
6.1.2 Liquid Saturation 74
6.2 Comparison with Conceptual Model 77
6.2.1 Matrix- versus Fracture-Dominated Flow in the Welded Units 77
6.2.2 Lateral Flow 79
7.0 Summary and Conclusions 82
References 89

List of Tables

Table 1.	Fracture density, porosity, permeability, and saturated hydraulic conductivity values for the hydrogeologic units.	8
Table 2.	Material properties specified in the one-dimensional simulations.	30
Table 3.	Material properties specified in the matrix-flow simulations.	39
Table 4.	Comparison of lateral flow and flux through the repository unit for the matrix-flow simulations.	41
Table 5.	Material properties specified in the fracture-flow simulations.	47
Table 6.	Comparison of computed, steady-state lateral flow and flux through the repository unit for the fracture-flow simulations.	49
Table 7.	Average computed flux through the repository unit as a function of the absolute permeability of the Fault Zone.	63
Table 8.	Summary of the effect of adding a second fault zone.	67
Table 9.	Distinguishing features of the six, two-dimensional flow simulations.	72
Table 10.	Comparison of the salient features of Matrix-flow Simulation #2 and Fracture Flow Simulation #2.	78
Table 11.	Comparison of the two-dimensional flow simulations in terms of lateral flow.	80

List of Figures

Figure 1.	Location map of Yucca Mountain.	2
Figure 2.	Vertical cross section through northern portion of Yucca Mountain (modified from Montazer and Wilson, 1984).	6
Figure 3.	Moisture-retention curves used to represent flow through the rock matrix of the hydrology units and Yucca Mountain (D. Hammermeister, USGS, personal communication, 1984).	12
Figure 4.	Comparison of straight-line approximation for extremely low values of matric potential with adsorption isotherm data of Herkelrath and O'Neal (1985) for the Topopah Spring welded unit.	14
Figure 5.	Relative-permeability curves used to represent flow through the rock matrix of the hydrologic units of Yucca Mountain.	15
Figure 6.	Characteristic curves representing fracture-flow conditions in the welded tuff units (Montazer and Harrold, 1985).	17
Figure 7.	Characteristic curves representing fracture-flow conditions in the Fault Zone (Montazer and Harrold, 1985).	19
Figure 8.	In situ measurements of water potential as a function of depth and time from borehole USW UZ-1 (Montazer et al., 1985).	20
Figure 9.	Variation in liquid saturation with depth measured on core samples and cuttings from borehole USW H1 (Weeks and Wilson, 1984).	21
Figure 10.	Boundaries of the flow region proposed in the conceptual model of Montazer and Wilson (1984).	24
Figure 11.	Hypothesized directions of liquid flow through the hydrogeologic units (modified from Montazer and Wilson, 1984).	25
Figure 12.	Discretized flow region for one-dimensional flow simulations.	29
Figure 13.	Profile of matric potential at steady state for the one-dimensional simulation in which Q = 0.001 mm/yr and for static conditions, Q = 0.	32
Figure 14.	Profiles of matric potential at steady state for one-dimensional simulations.	34
Figure 15.	Profiles of liquid saturation at steady state for one-dimensional simulations.	35
Figure 16.	Discretized flow region used in the two-dimensional flow simulations.	37

Figure 17.	Vector plot of computed mass flux through the flow system at steady state for Matrix-Flow Simulation #1.	40
Figure 18.	Contour diagram of the computed matric-potential distribution at steady state for Matric-Flow Simulation #1.	43
Figure 19.	Contour diagram of the computed matric-potential distribution at steady state for Matrix-Flow Simulation #2.	43
Figure 20.	Contour diagram of the computed liquid-saturation distribution at steady state for Matrix-Flow Simulation #2.	44
Figure 21.	Contour diagram of the computed liquid-saturation distribution at steady state for Matrix-Flow Simulation #2.	44
Figure 22.	Outflow across the water table as a function of time for Matrix-Flow Simulation #1.	45
Figure 23.	Vector plot of computed mass flux through the flow system at steady state for Fracture-Flow Simulation #1.	48
Figure 24.	Contour diagram of the computed matric-potential distribution at steady state for Fracture-Flow Simulation #1.	51
Figure 25.	Contour diagram of the computed matric-potential distribution at steady state for Fracture-Flow Simulation #2.	51
Figure 26.	Contour diagram of the computed liquid-saturation distribution at steady state for Fracture-Flow Simulation #1.	52
Figure 27.	Contour diagram of the computed liquid-saturation distribution at steady state for Fracture-Flow Simulation #2.	52
Figure 28.	Qualitative representation of the relationship between permeability, matric potential, and liquid saturation for a "combined" fracture-matrix medium (modified from Montazer and Wilson, 1984, Figure 6).	53
Figure 29.	Hypothetical combined curve used in Fracture-Matrix Flow Simulation #1 (modified from Montazer and Wilson, 1984, Figure 6).	55
Figure 30.	Contour diagram of the computed matric-potential distribution at steady state for Fracture-Matrix Flow Simulation #1.	56
Figure 31.	Combined curve used in Fracture-Matrix Flow Simulation #2 (Montazer and Wilson, 1984, Figure 6).	57
Figure 32.	Vector plot of the computed mass flux through the flow system at steady state for Fracture-Matrix-Flow Simulation #2.	59
Figure 33.	Contour diagram of the computed Matric-potential distribution at steady state for Fracture-Matrix Flow Simulation #2.	60

Figure 34.	Contour diagram of the computed liquid-saturation distribution at steady state for Fracture-Matrix Flow Simulation #2.	61
Figure 35.	Vector plot of the computed mass flux through the flow system at steady state for the case in which the absolute permeability of the Fault Zone is reduced by three orders of magnitude.	64
Figure 36.	Vector plot of the computed mass flux through the flow system at steady state for the case of two fault zones.	66
Figure 37.	Contour diagram of the computed matric-potential distributions at steady state for a coarse mesh and a fine mesh.	69
Figure 38.	Contour diagram of the computed liquid-saturation distributions at steady state for a coarse mesh and a fine mesh.	70
Figure 39.	Location of vertical section A-A' corresponding to the location of borehole USW UZ-1.	73
Figure 40.	Comparison of the profiles of calculated matric potential along A-A' for the six 2-dimensional simulations.	75
Figure 41.	Comparison of the profiles of calculated saturation along A-A' for the six 2-dimensional simulations.	76

Acknowledgements

This work was carried out under U.S. Department of Energy Contract No. DE-AC03-76SF00098 via the DOE-Nevada Office in cooperation with USGS-Denver; project direction provided by B. Wilson. The authors are grateful to K. Pruess, who provided the numerical code TOUGH prior to its release for general use. Critical review of this work by B. Wilson, D. Hoxie, Y. Tsang, S. Benson, K. Pruess, J. Wang, and S. Loomis is appreciated. The authors express their thanks to L. Fairbanks, C. Joy, M. Bodvarsson, and P. Fuller for their technical assistance.

1.0 INTRODUCTION

In the late 1970's, the U.S. Department of Energy began funding research to determine the feasibility of constructing a geologic repository for storing high-level radioactive waste in the tuff sequence at the Nevada Test Site. The resulting investigations have focused on Yucca Mountain, located along the western border of the Nevada Test Site (see Figure 1). The U.S. Geological Survey (USGS) has been conducting hydrologic investigations at this site as part of the Nevada Nuclear Waste Storage Investigations, administered by the Nevada Operations Office of the Department of Energy. In cooperation with the USGS, numerical studies of the natural state of the groundwater-flow system have been performed at Lawrence Berkeley Laboratory to examine the general groundwater-flow patterns predicted on the basis of the available data and to aid in the evaluation of a conceptual hydrogeologic model of the site. This report presents the approach and results of these preliminary numerical studies.

The hydrogeology at Yucca Mountain is characterized by flow through heterogeneous, anisotropic, partially saturated, fractured rock in an arid environment. The mountain is composed of fault blocks with alternating layers of welded and nonwelded tuff units. The welded units are highly fractured, with a fracture density ranging from 8 to 40 fractures/m^3 ; the nonwelded units have a fracture density ranging from 1 to 3 fractures/m^3 (Scott et al., 1983). At Yucca Mountain, the unsaturated zone is 500 to 750 m thick (Robison, 1984). Recharge to the saturated zone through the unsaturated zone at Yucca Mountain is estimated to be less than 4.5 mm/yr, and probably less than 0.5 mm/yr (Montazer and Wilson, 1984).

For the purpose of predicting the migration of radionuclides from buried waste at Yucca Mountain, reliable estimates of the magnitude and direction of groundwater flow in the region are needed; that is, the natural state of the groundwater-flow system must

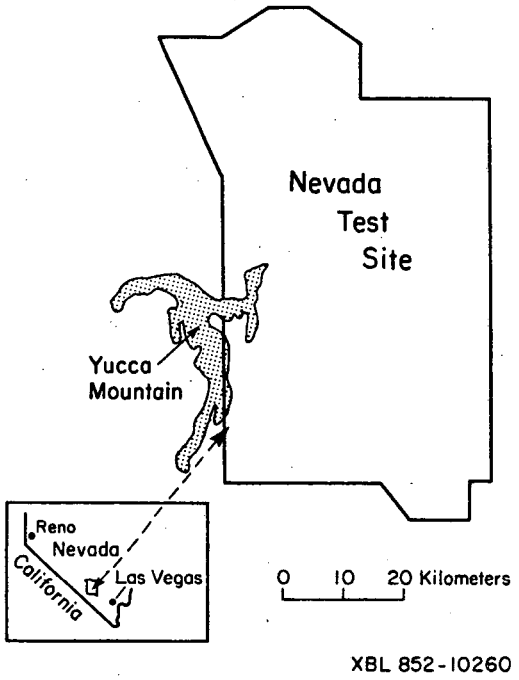

Figure 1. Location map of Yucca Mountain.

be understood. Montazer and Wilson (1984) proposed a conceptual model for this purpose, based on their interpretation of the available data and the principles of groundwater flow through partially saturated material. They hypothesize flow patterns based on the combined effects of fracture-matrix interactions, capillary barriers, hysteresis, and vapor transport. Ideas contained in the conceptual model are expected to be confirmed, revised, or rejected as results become available from ongoing field studies, experimental studies, and theoretical studies, such as the one presented in this report.

Theoretical studies of the Yucca Mountain site necessitate the use of numerical models because of the complexity of the geology and the highly nonlinear equations that govern transport in unsaturated materials. A comprehensive theoretical model of the site would include the transient, three-dimensional flow water, heat and air through both the fractures and the rock matrix. In addition, the spatial variability of the material properties within each unit would be modeled. However, initial theoretical studies, such as the one presented here, should be tailored to the available data and be kept as simple as possible. For this reason, steady-state, two-dimensional non-hysteretic flow of liquid water through the system was chosen for analysis. The flow of heat, water vapor, and air was neglected. Fractures were not modeled in a discrete manner; instead, for the fractured units, characteristic curves that theoretically incorporate the effects of fractures on unsaturated groundwater flow were used. A series of minor faults present along the eastern boundary of Yucca Mountain were modeled as a single hydrogeologic unit with properties believed to be representative of a broad, permeable fault zone. And, as a final simplication, each hydrogeologic unit was assumed to be homogeneous. By beginning with the simplest possible model, the available data and complexities of the system may be incorporated in a step-wise fashion so that at any given time, the numerical model can produce the best current estimate of the natural state of the system.

In this report, the hydrogeology at the Yucca Mountain site is briefly described in terms of the available data and in terms of a proposed conceptual model. The

mathematical model used to study the flow system is briefly described. Finally, results from one- and two-dimensional flow simulations are presented and discussed.

2.0 AVAILABLE DATA

Hydrogeologic data have been obtained from numerous boreholes and other sources at the Yucca Mountain site. For the purposes of this study, these data were grouped into two categories. In the first group are those data that characterize the material properties of the hydrogeological units, namely, the fracture density, the porosity, the saturated hydraulic conductivity, and the curves relating matric potential, liquid saturation, and relative permeability. In the second group are those data that describe the natural state of the hydrogeologic system, namely, precipitation data and profiles showing the variation with depth of the water potential, and liquid saturation. These two groups of data are presented following a brief description of the hydrogeologic setting of the Yucca Mountain site.

2.1 General Hydrogeologic Setting

Yucca Mountain is a north-trending, fault-block ridge composed of volcanic tuff units, located in the Basin and Range Province of Nevada. The volcanic rocks range in age from 11 to 15 million years and were erupted from caldera complexes north of Yucca Mountain (Carr et al., 1984). A detailed description of the geology of the site is given by Scott et al. (1983) and Scott and Bonk (1984); features relevant to the present study are summarized below.

Figure 2 is a vertical section through the northern part of the ridge. As shown, Yucca Mountain is bounded to the west by a steeply-dipping, major normal fault and along the east by a series of minor normal faults. The structural blocks dip 5 to 10 degrees eastward (Scott and Bonk, 1984). A distinct set of north-northeast striking fractures has been mapped at the surface and appear to be non-stratabound, tectonic features; randomly distributed, stratabound cooling joints have also been mapped (Scott

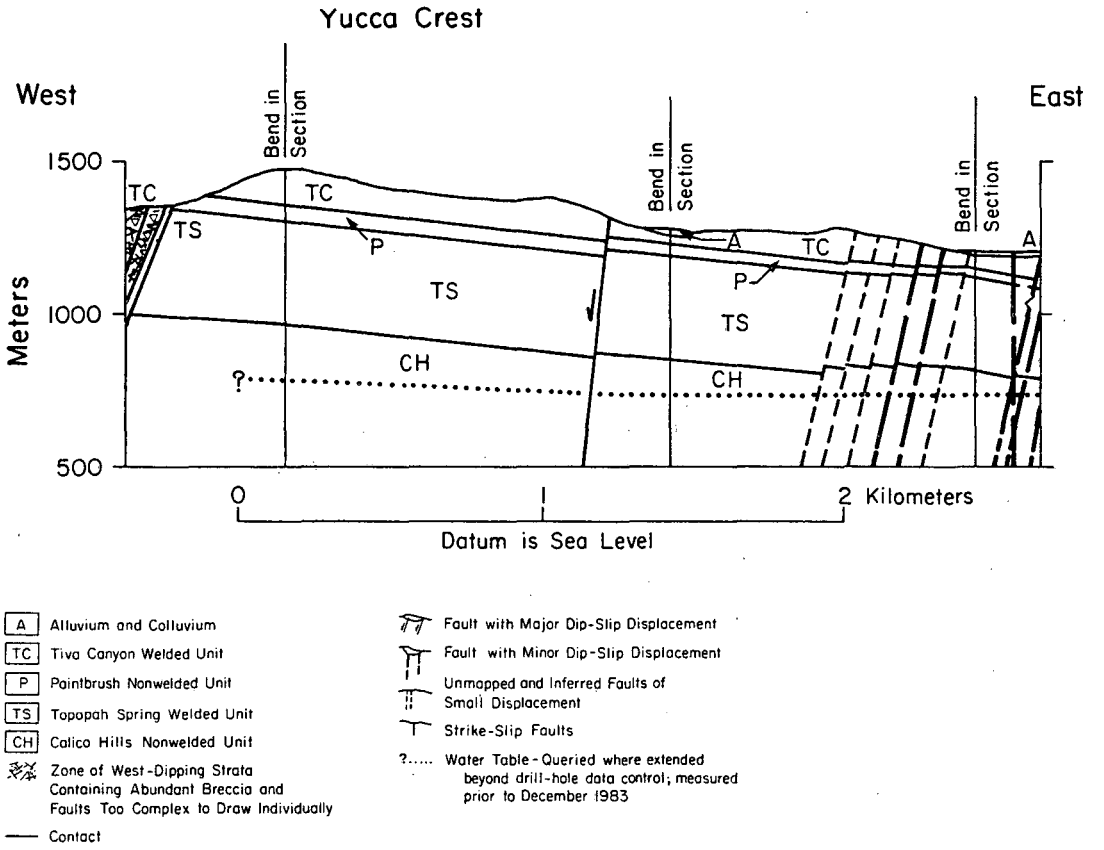

Figure 2. Vertical cross section through northern portion of Yucca Mountain (modified from Montazer and Wilson, 1984).

et al., 1983).

Beneath the northern section of the mountain, the unsaturated zone includes the following hydrogeologic units, as defined by Montazer and Wilson (1984): the Tiva Canyon welded unit, the Paintbrush nonwelded unit, the Topopah Spring welded unit, and the Calico Hills nonwelded unit. The Topopah Spring welded unit is the potential repository unit. The hydrogeologic units are differentiated on the basis of physical properties that control the occurrence and flow of water through the Yucca Mountain system. In general, the welded units are ash-flow tuffs with high fracture densities, low matrix porosities, and low matrix permeabilities. The nonwelded units are bedded tuffs and ash-flow tuffs with low fracture densities, high matrix porosities, and, in general, relatively high matrix permeabilities. In addition to these hydrogeologic units, the series of faults bounding Yucca Mountain to the east were grouped into an informal unit called the Fault Zone for the purpose of numerical modeling. In this report, the Fault Zone is assumed to be highly fractured and transmissive in the vertical direction.

The regional water table is 500 to 750 m below the ground surface (Robison, 1984). The majority of the recharge to the regional saturated groundwater system occurs in the mountain ranges to the north of Yucca Mountain and regional discharge areas are to the southwest in parts of the Armagosa Desert and Death Valley (Waddell et al., 1984). The general regional flow direction in the saturated zone, therefore, is south-southeast (Robison, 1984).

2.2 Hydraulic Properties of the Units

The fracture density, matrix porosity, matrix permeability, and saturated hydraulic conductivity are listed for each unit in Table 1. These values represent the best estimates at the present time. Note that only single values are given although there is substantial variation in these parameters within each unit. Because parts of the Calico Hills nonwelded unit have undergone zeolitization, it has been differentiated into two distinct

Table 1. Fracture density, porosity, permeability, and saturated hydraulic conductivity values for the hydrogeologic units.

Unit Name	[1]Fracture Density (fractures/m^3)	[2]Matrix Properties			
		Porosity	Absolute Horizontal Permeability (m^2)	Saturated Horizontal Hydraulic Conductivity (m/s)	Anisotropy Ratio (Horizontal/Vertical)
Tiva Canyon welded unit	10-20	0.12	2.4×10^{-18}	2.3×10^{-11}	1
Paintbrush nonwelded unit	1	0.46	1.0×10^{-14}	9.8×10^{-8}	10
Topopah Spring welded unit	8-40	0.14	3.9×10^{-18}	3.8×10^{-11}	1
Calico Hills (vitric) nonwelded unit	2-3	0.37	5.0×10^{-15}	4.9×10^{-8}	10
Calico Hills (zeolitic) nonwelded unit	2-3	0.33	9.3×10^{-18}	9.1×10^{-11}	1

Fault Zone

fracture porosity = 0.05

absolute horizontal permeability (m_2) = 1.0×10^{-12}

saturated horizontal hydraulic conductivity = 9.8×10^{-6} (m/s)

anisotropy ratio (horizontal/vertical) = 0.02

References

1 Scott et al. (1983)

2 Montazer and Wilson (1984)

units, Calico Hills (vitric) and Calico Hills (zeolitic). The zeolitic portion has a relatively low permeability and contains a discontinuous, vertical fracture network. The Paintbrush nonwelded unit and the Calico Hills (vitric) nonwelded unit are assumed to be anisotropic due to bedded tuff layers. Data are not yet available to quantify the anisotropy ratio for these two units; it was assumed that the permeability in the horizontal direction is ten times that in the vertical direction. The Fault Zone is highly fractured and assigned transmissive properties. It is also assumed to be anisotropic, with the absolute permeability in the vertical direction fifty times that in the horizontal direction. The value of the absolute horizontal permeability assigned to the Fault Zone corresponds to air-permeability tests performed in highly fractured welded tuff (Montazer et al., 1985).

In addition to the properties listed in Table 1, the analysis of liquid flow through unsaturated media requires knowledge of the relationships between matric potential, ϕ_m, liquid saturation, S_l, and hydraulic conductivity, K, for each hydrogeologic unit. This information is commonly expressed in the form of two curves. The first, the moisture-retention curve, describes the dependence of liquid saturation on matric potential. Liquid saturation, S_l, is given by:

$$S_l = \frac{\theta}{n}$$

where θ = volumetric water content and n = porosity. Matric potential, ϕ_m, is defined as :

$$\phi_m = \rho_l \; g \; \psi - p_o \tag{1}$$

where ρ_l = liquid density [M/L^3], g = gravitational constant [L/T^2], ψ = pressure head [L], and p_o = air pressure [M/LT^2]. In this report, air pressure is assumed to be atmospheric and refers to gage pressure, so that $p_o = 0$. As defined in Equation 1, ϕ_m has units of pressure and is negative, since the pressure head is negative in the unsaturated zone.

The second curve, the relative-permeability curve, relates the liquid saturation to the relative permeability of the liquid phase, $k_{r,l}$. The relative permeability, expressed as a function of S_l, is given by:

$$k_{r,l}(S_l) = \frac{k_r(S_l)}{k_a}$$

where k_a is the absolute (saturated) permeability, and $k_r(S_l)$ is the permeability to liquid flow at a given liquid saturation. The hydraulic conductivity, K, can then be obtained from the following equation:

$$K = \frac{k_{r,l}(S_l)k_a \rho_l \ g}{\mu_l}$$

where μ_l = liquid viscosity.

The moisture-retention curve and relative-permeability curve are collectively known as the characteristic curves of a material. A detailed discussion of characterisitic curves can be found in standard soil physics texts, such as Hillel (1980). Two types of characteristic curves were used in this study and are described below. First are those that represent flow through the rock matrix and second are those that represent flow through fractured media.

2.2.1 Matrix Characteristic Curves

For flow through rock matrix, moisture-retention data are available but relative-permeability data are not. In fact, techniques to measure the relative-permeability for air-water systems in consolidated rock have yet to be firmly established. In lieu of these data, methods developed for unconsolidated soils that predict the relative-permeability curve, given moisture-retention data, were used. The applicability of these methods to consolidated rock will remain at issue until measurements are available for validation.

The methods most often used to predict relative-permeability curves from moisture-retention data are those of Millington and Quirk (1961), Brooks and Corey

(1964), and van Genuchten (1980). The van Genuchten method was chosen for this investigation because it gives continuous, closed form analytical expressions for both curves. The methodology is fully described by van Genuchten (1980) and essentially involves adjusting three parameters until an analytical expression provides the best-possible fit to the measured moisture-retention curve. These parameters are then used in another analytical expression to predict the relative-permeability curve. The expressions for these curves are:

$$S_l(\,|\,\phi_m\,|\,) = S_{r,l} + \frac{S_{s,l} - S_{r,l}}{\left[1 + (\alpha\,|\,\phi_m\,|\,)^n\right]^m} \tag{2}$$

$$k_{r,l}(\,|\,\phi_m\,|\,) = \frac{\left\{1 - (\alpha\,|\,\phi_m\,|\,)^{n-1}\left[1 + (\alpha\,|\,\phi_m\,|\,)^n\right]^{-m}\right\}^2}{\left[1 + (\alpha\,|\,\phi_m\,|\,)^n\right]^{m/2}} \tag{3}$$

where

$S_{r,l}$ = residual liquid saturation
$S_{s,l}$ = satiated liquid saturation
α,n,m = vanGenuchten parameters

Note that the van Genuchten expression uses the absolute value of the matric potential. The satiated liquid saturation refers to the maximum obtainable saturation. Theoretically, $S_{s,l}$=1.0; however in practice, $S_{s,l}$ may be slightly less than unity because it is extremely difficult to saturate a rock sample fully.

The moisture-retention curves used to represent liquid flow through rock matrix for the different units are shown in Figure 3. There are three items to note in regard to this set of curves:

1. The van Genuchten method works well when the moisture-retention curve is roughly "S"-shaped, as in Figures 3a, 3b and 3c. The data for the Calico Hills (zeolitic) nonwelded unit did not conform; instead, the curves were approximated with linear segments, as shown in Figure 3d.

3a. Paintbrush nonwelded unit.

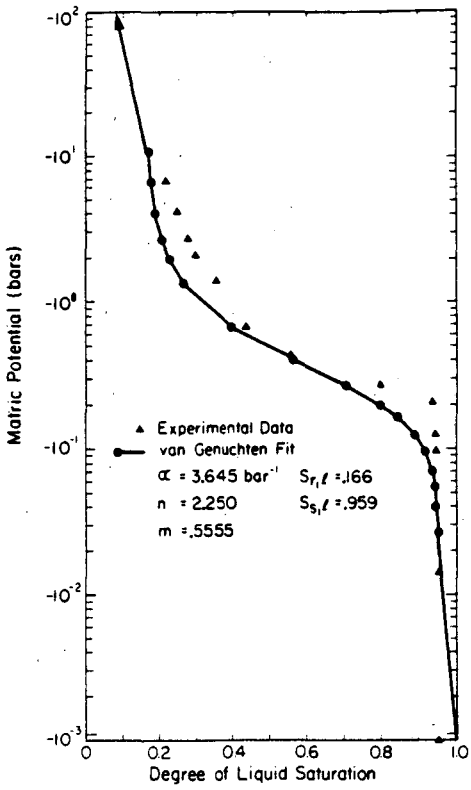

3b. Topopah Spring welded unit.

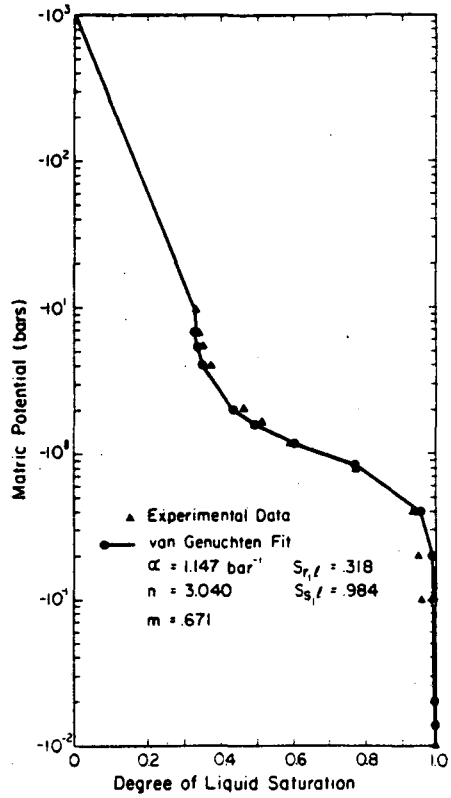

3c. Calico Hills (vitric) nonwelded unit.

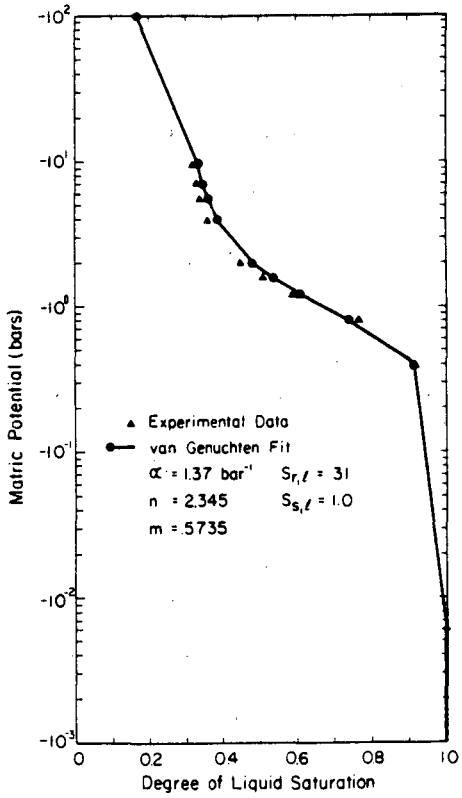

3d. Calico Hills (zeolitic) nonwelded unit.

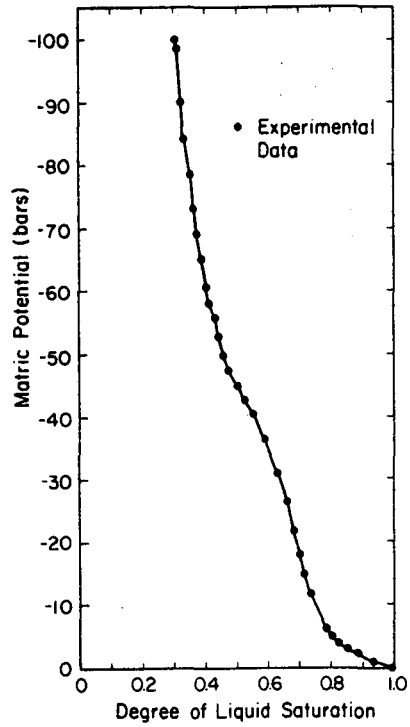

Figure 3. Moisture-retention curves used to represent flow through the rock matrix of the hydrology units and Yucca Mountain (D. Hammermeister, USGS, personal communication, 1984).

2. Measurements to construct the moisture-retention curve for the Calico Hills (vitric) nonwelded unit were not initially available so that measurements made on samples of the Topopah Spring welded unit were used to approximate it. The moisture-retention data are now available and are reported by Peters et al. (1984).

3. The moisture-retention data generally did not encompass the full range of liquid saturation ($S_l = 0$ to $S_l = 1$) as required by the iterative solution technique used in the numerical model. For cases in which $S_{s,l} < 1$ (Figure 3a and 3b), the moisture-retention curve was extended with a straight line to $S = 1$, as shown. All curves shown in Figure 3 were extended to $S_l = 0$ using a straight-line approximation between the point ($S_l = 0$, $\phi_m = -1000$ bars) and the point on the moisture-retention curve where $\phi_m = -10$ bars. During the latter stages of this work, this approximation was compared with data obtained from experiments on samples of Topopah Spring welded unit designed to measure liquid saturation for values of matric potential between -10 and -10,000 bars from adsorption isotherm data (Herkelrath and O'Neal, 1985). The comparison is shown in Figure 4. However, as illustrated in a later section, the numerical results show that the matric potential at steady state generally exceeds -10 bars when matrix flow is modeled. Hence the linear approximation at low liquid saturations has little effect on the results.

Based on the curves shown in Figure 3, relative-permeability curves were developed to represent matrix flow. These are shown in Figure 5. There are two items to note in regard to this set of curves:

1. It was necessary to modify the curves predicted by the van Genuchten Method (Figures 5a, 5b and 5c), because the solution oscillates when the expression inside the braces in Equation 3 becomes negative, i.e., when

$$(\alpha \mid \phi_m \mid)^{n-1} \left[1 + (\alpha \mid \phi_m \mid)^n\right]^{-m} > 1$$

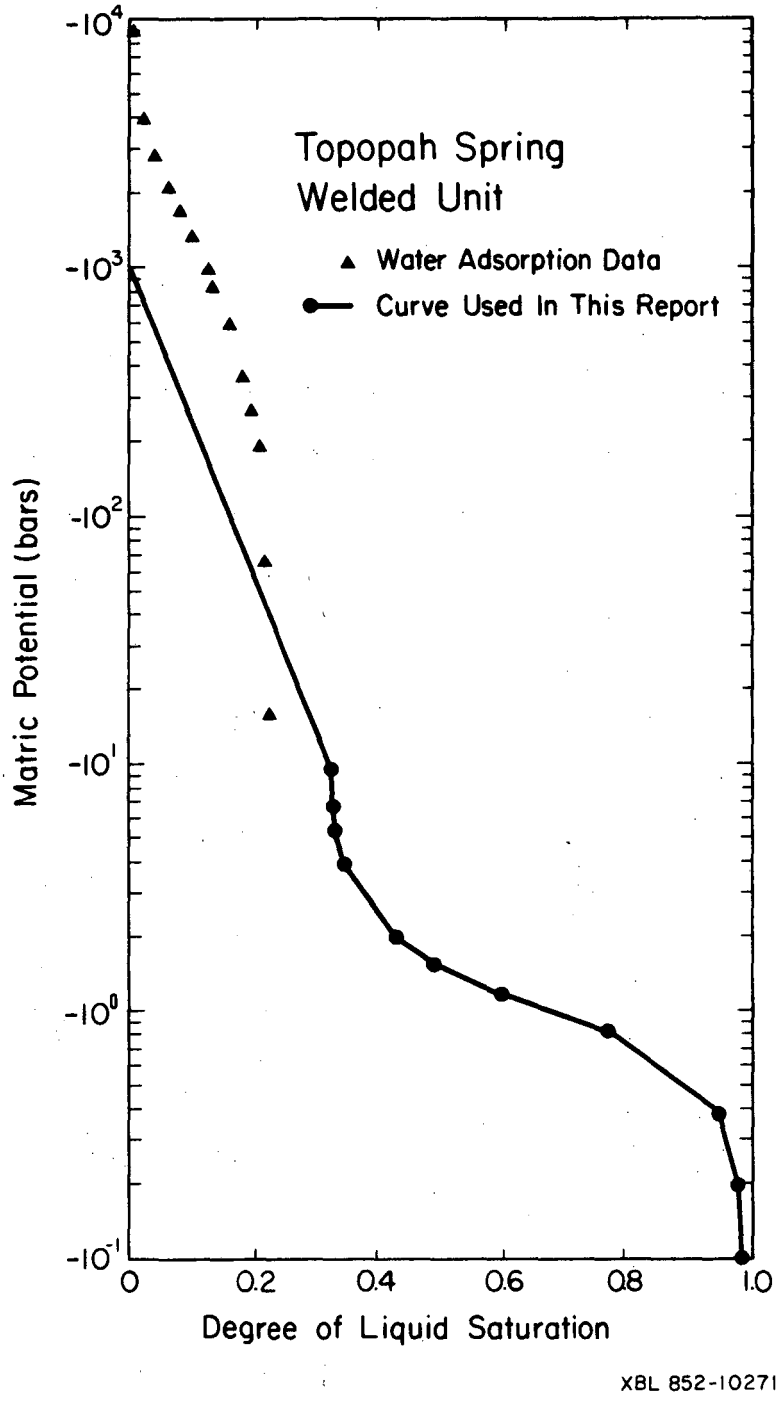

Figure 4. Comparison of straight-line approximation for extremely low values of matric potential with adsorption isotherm data of Herkelrath and O'Neal (1985) for the Topopah Spring welded unit.

5a. Paintbrush nonwelded unit.

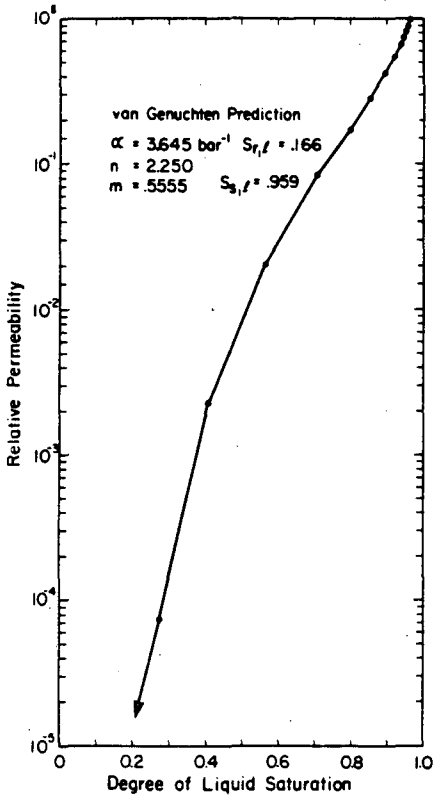

5b. Topopah Spring welded unit.

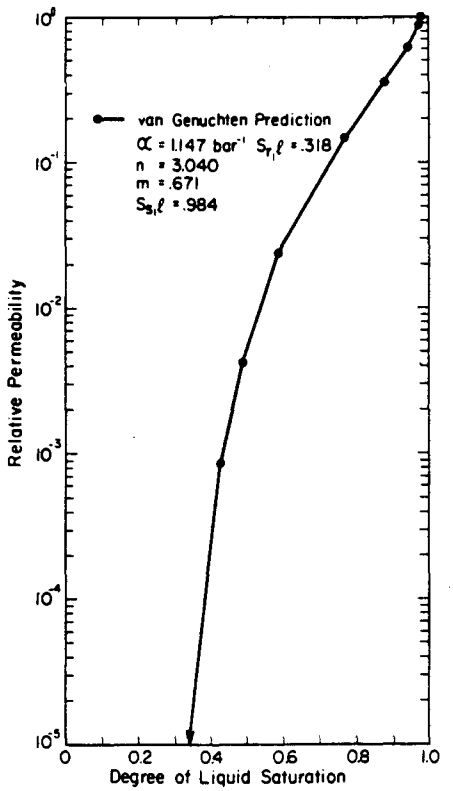

5c. Calico Hills (vitric) nonwelded unit.

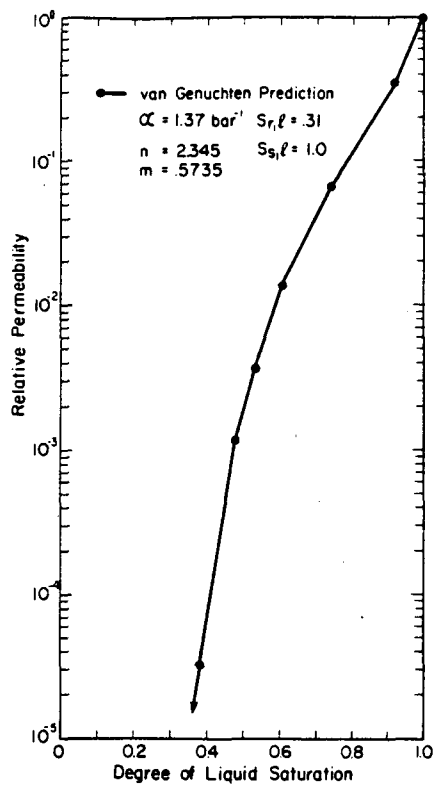

5d. Calico Hills (zeolitic) nonwelded unit.

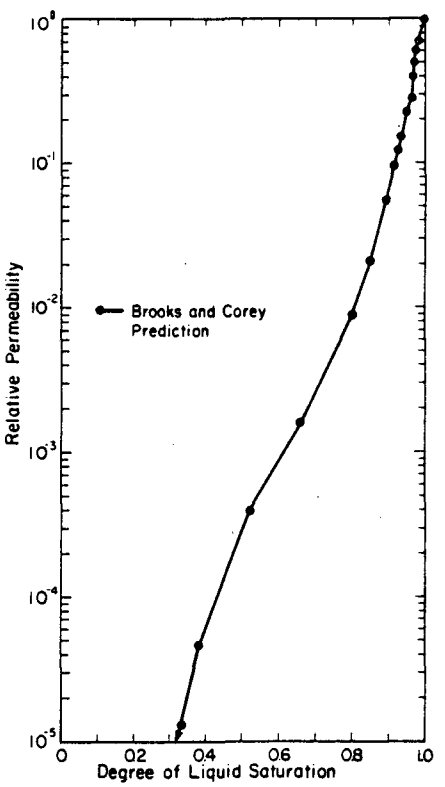

Figure 5. Relative-permeability curves used to represent flow through the rock matrix of the hydrologic units of Yucca Mountain.

For example, for the Topopah Spring welded unit, n = 3.04, m = 0.671 and α = 1.47 and the solution oscillates for $|\phi_m| > 10.5$ bar, or liquid saturations less than 0.322. Therefore, a log-linear approximation was chosen for $k_{r,l} < 10^{-4}$ for all relative permeability curves predicted by this method (Figure 5a, 5b and 5c).

2. Because the van Genuchten analysis could not be applied to the Calico Hill (zeolitic) nonwelded unit, the points shown in Figure 5d represent a prediction based on the Brooks and Corey method (D. Hoxie, USGS, written communication, 1984).

2.2.2 Fracture Characteristic Curves

Characteristic curves describing unsaturated flow through fractured rock have yet to be developed based on experimental data. However, theoretical models have been proposed from which the relationships between fracture aperture, matric potential, liquid saturation and permeability were calculated based on the principles of flow through parallel plates of varing aperture (Montazer and Wilson, 1984; Wang and Narasimhan, 1985; Montazer and Harrold, 1985). Development of the curves used in this report is described by Montazer and Harrold (1985). Figure 6 shows the curves used to represent fracture flow through the welded units. The curves show an assumed air-entry value of -1.34 bars; that is, suction equivalent to -1.34 bars must be applied for air to first enter the fractured rock during the drainage process. Data are not available to quantify the true air-entry value of the welded units. From the capillary-rise equation (Hillel, 1980), one can calculate that an air-entry value of -1.34 bars corresponds to an effective fracture aperture of 0.3 μm. This appears to be an extremely small value for fracture aperture, but it may provide a reasonable lower bound since it is an order of magnitude greater than the mean pore diameter for samples of the welded tuff units as reported by Peters et. al (1984). The curves shown in Figure 6, therefore, represent a fractured rock dominated by microfractures. The effect of increasing the air-entry value, and hence the effective aperture, is examined in the numerical simulations.

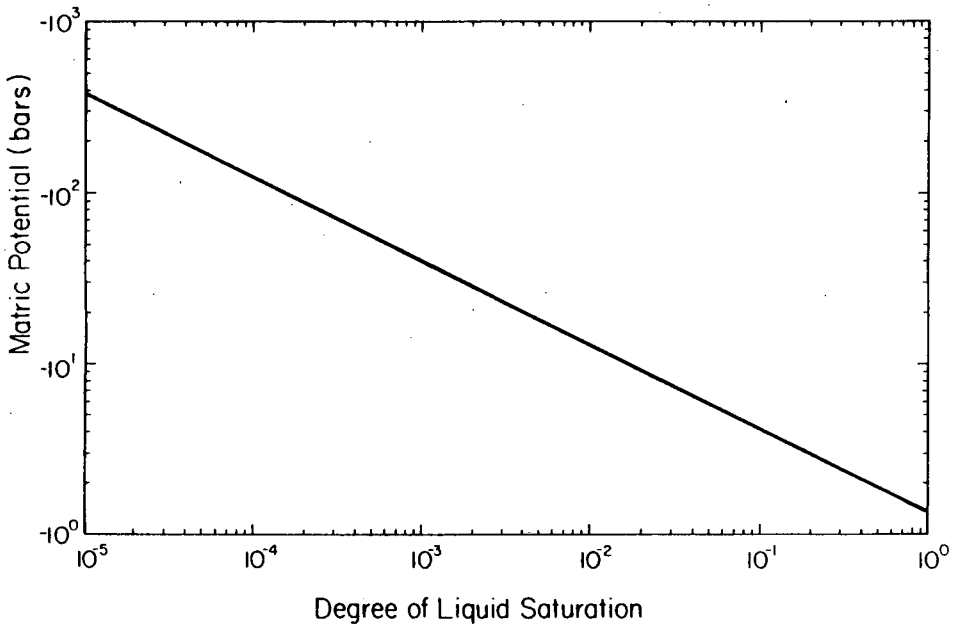

6a. Moisture-retention curve.

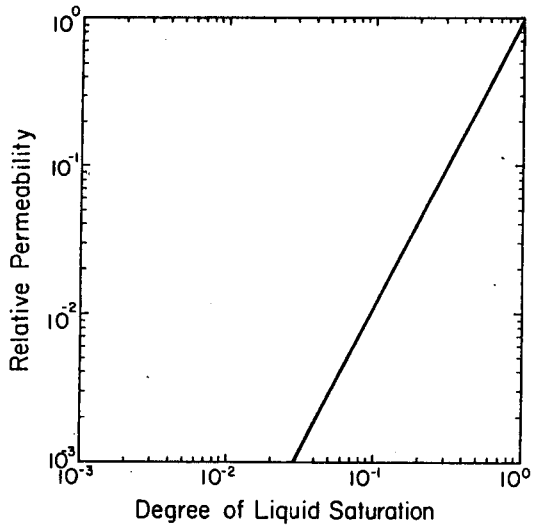

6b. Relative-permeability curve.

Figure 6. Characteristic curves representing fracture-flow conditions in the welded tuff units (Montazer and Harrold, 1985).

Flow through the Fault Zone is also represented as fracture flow; the theoretical fracture curves for this unit are given in Figure 7. The liquid saturation that appears in the fracture characteristic curves refers to fracture saturation, i.e, the volume of water contained in the fractures per fracture porosity. The fracture porosity is the ratio of the fracture volume to the total rock volume. The air-entry value for the Fault Zone is assumed to be -0.1 bar and is intended to reflect greater effective apertures due to faulting.

2.3 Natural-State Data

2.3.1 Precipitation Data

At present, estimates of the average precipitation at Yucca Mountain are based upon indirect methods because records of direct precipitation are not long enough to provide reliable estimates. Winograd and Thordarson (1975) present a regional map from which precipitation at Yucca Mountain is estimated to be between 100 and 150 mm/yr. From relationships between altitude and precipitation developed by Quiring (1983), Montazer and Wilson (1984) estimate precipitation to be about 150 mm/yr.

2.3.2 Profiles of Water Potential and Liquid Saturation

Figure 8 shows in-situ measurements of water potential as a function of depth from borehole USW UZ-1 (Montazer et al., 1985). Water potential is defined as the sum of matric potential and osmotic potential. Preliminary measurements indicate that the osmotic potential is generally a negligible component, between 0 and -2 bars, (D. Hammermeister, USGS, personal communication, 1985) so that the data in Figure 8 can be used as an approximate indication of general trends in the matric potential. Figure 8 indicates that the matric potential in the Topopah Spring welded unit generally decreases with depth and ranges between -1 bar and -10 bars.

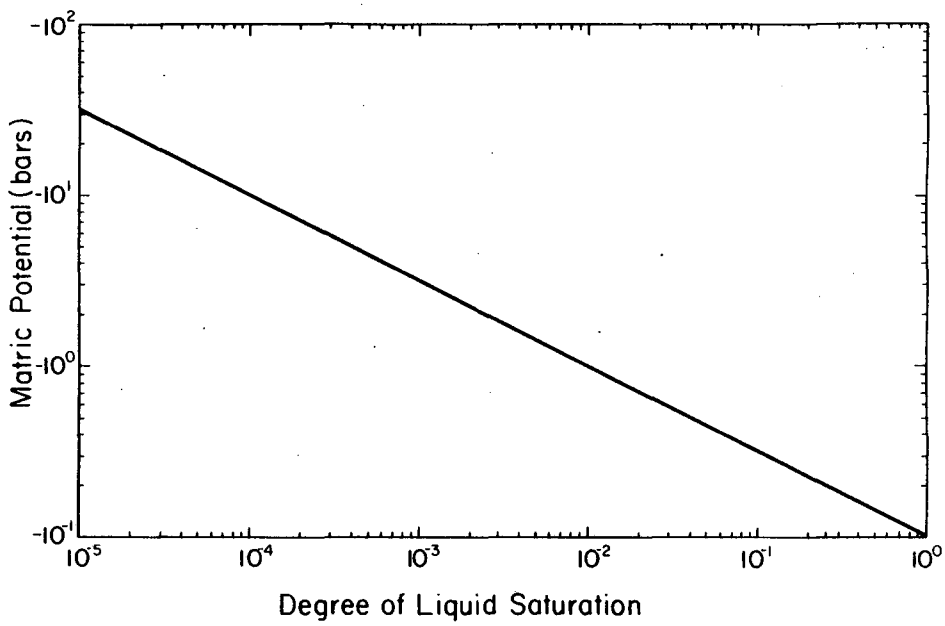

7a. Moisture-retention curve.

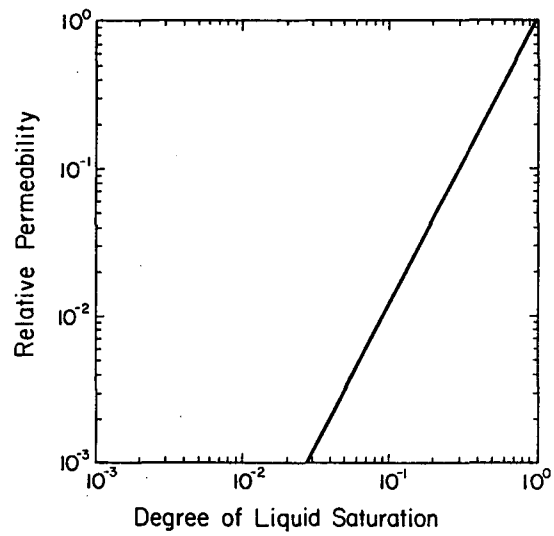

7b. Relative-permeability curve.

Figure 7. Characteristic curves representing fracture-flow conditions in the Fault Zone (Montazer and Harrold, 1985).

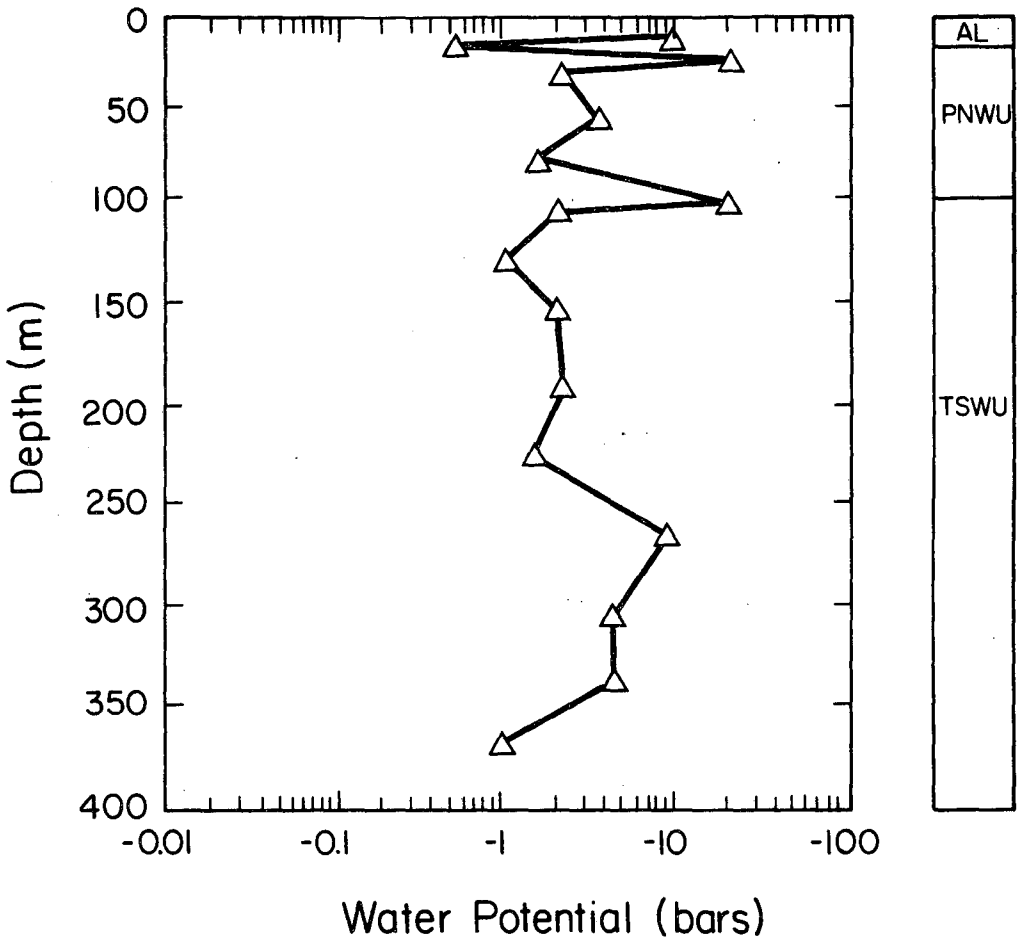

AL = Alluvium
PNWU = Paintbrush Non welded Unit
TSWU = Topopah Spring Welded Unit

XBL 8510-12343

Figure 8. In situ measurements of water potential as a function of depth and time from borehole USW UZ-1 (Montazer et al., 1985).

Figure 9 shows the variation in liquid saturation measured on core and cutting samples from a borehole near USW UZ-1, borehole USW H1 (Weeks and Wilson, 1984). These data indicate that the liquid saturation within the Topopah Spring welded unit ranges between 0.30 and 0.80, with an average of approximately 0.65. Figure 9 also shows a general increase in liquid satuation with depth in the repository unit. It should be noted that the observed liquid-saturation data and matric-potential data can not both be matched using the characteristic curves presented earlier. The reason is that the characteristic curves show increasing matric potential with increasing liquid saturation, whereas the field data suggest decreasing matric potential with increasing liquid saturation with depth in the Topopah Spring welded unit. This discrepancy may be due to heterogeneity within the Topopah Spring welded unit as the measured values of matric potential and liquid saturation are extremely sensitive to variations in bulk density and changes in the pore-size distribution.

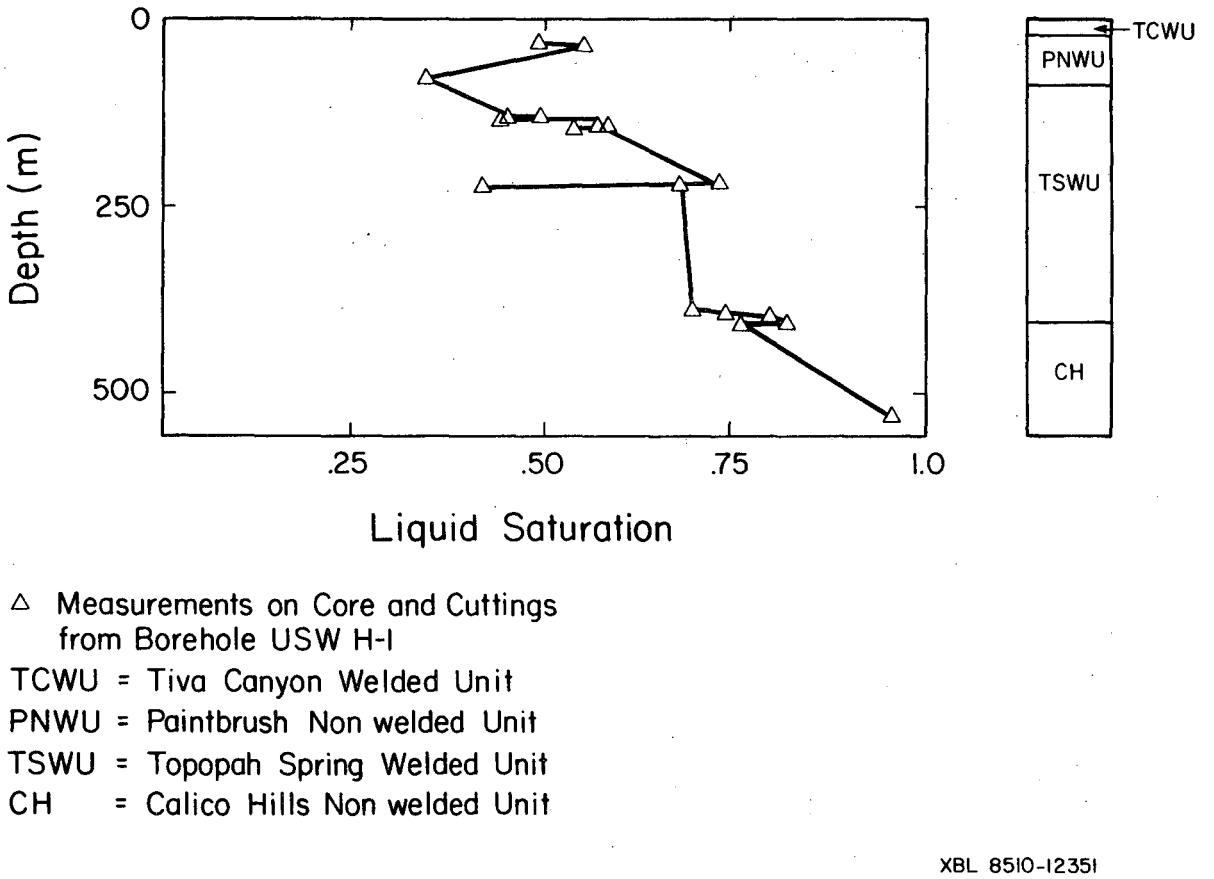

Figure 9. Variation in liquid saturation with depth measured on core samples and cuttings from borehole USW H1 (Weeks and Wilson, 1984).

3.0 CONCEPTUAL MODEL

A conceptual model of liquid flow through the unsaturated zone beneath Yucca Mountain was proposed by Montazer and Wilson (1984); some of the salient features are outlined in this section, namely, the boundary conditions and the inferred liquid flow paths through the system. The conceptual model is a working hypothesis; the preliminary nature is due to: (a) the scarcity of data, (b) the fact that flow through heterogeneous, unsaturated, fractured rock systems in arid environments not yet fully understood, and (c) the lack of well-established field techniques to characterize such systems.

The boundaries of a simplified, two-dimensional flow region are shown schematically in Figure 10. The unsaturated flow system is bounded by the land surface and the water table. In this report, a flow region typical of the northern part of the central mountain block is considered where the water table is within the Calico Hills nonwelded unit. Beneath the southern part of the mountain, the water table occurs in the Crater Flat unit underlying the Calico Hills nonwelded unit. The lateral extent of the flow system has not been determined conclusively. The vertical boundaries have been tentatively placed along the faults that bound the region. As indicated in Figure 10, segments of the vertical boundaries adjacent to welded units are assumed to be impermeable; those adjacent to nonwelded units are assumed to represent sources or sinks.

Annual precipitation at the site is estimated to be 150 mm/yr. Of this, about 0.5 to 4.5 mm/yr is believed to recharge the saturated zone through the unsaturated zone. This estimate is based on indirect techniques, including water-budget studies and analyses of geothermal-heat flux.

The hypothesized directions of liquid flow through the hydrogeologic units are shown in Figure 11. For the sake of simplicity, only the central block beneath Yucca Mountain is shown since the flow patterns are assumed to be identical in the blocks to the east. In addition, for simplicity of expression, the inferred flow patterns are described as if they were a true expression of the facts; in reality, all conceptual models

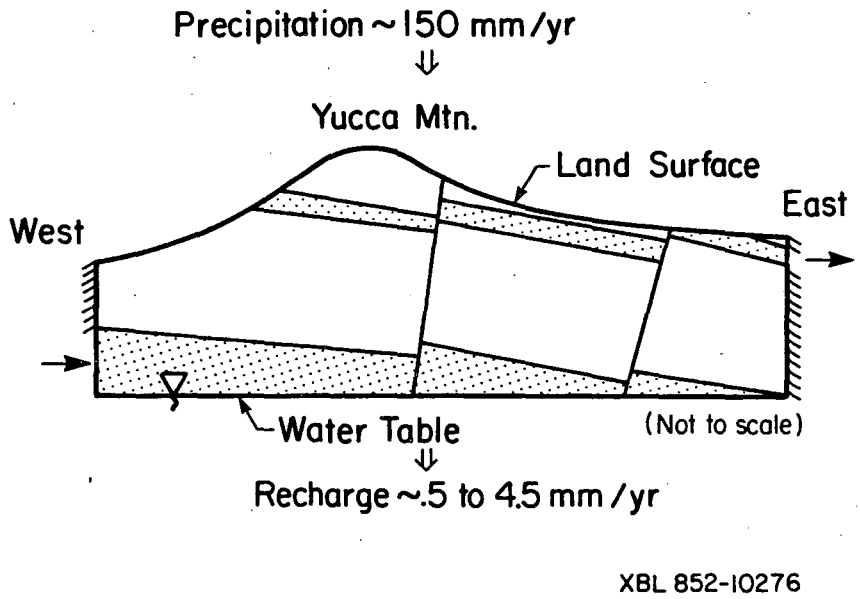

Figure 10. Boundaries of the flow region proposed in the conceptual model of Montazer and Wilson (1984).

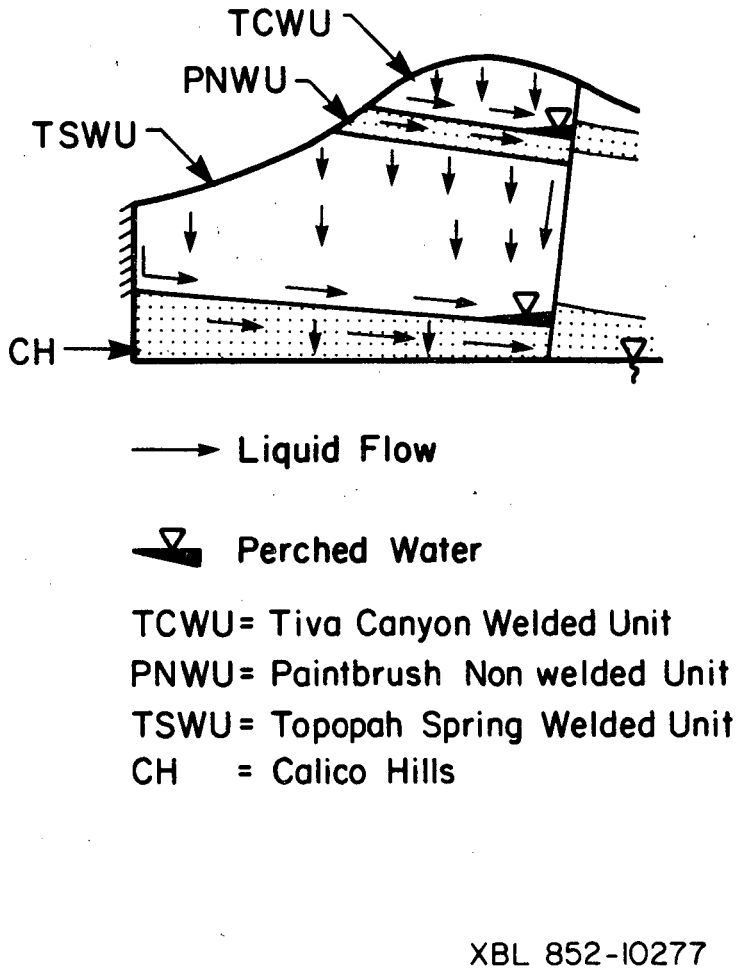

Figure 11. Hypothesized directions of liquid flow through the hydrogeologic units (modified from Montazer and Wilson, 1984).

of the Yucca Mountain system are, at this point, conjectural. As indicated in Figure 11, infiltration from the ground surface flows vertically through the fractures of the Tiva Canyon welded unit; a small part of the water diffuses into the matrix. Lateral flow occurs at the contact between the Tiva Canyon welded unit and the Paintbrush nonwelded unit, due to capillary-barrier effects, described in Montazer and Wilson (1984). Within the Paintbrush nonwelded unit, lateral flow occurs due to anisotropy, capillary-barrier effects, and the fact that the saturated hydraulic conductivity is 2 to 3 orders of magnitude greater than the saturated matrix hydraulic conductivity of the underlying Topopah Spring welded unit. Water moves vertically through the Topopah Spring welded unit in the matrix and as sheet flow along fractures in the upper part of the unit, with eventual diffusion into the matrix in the lower part of the unit. Lateral flow is postulated at the base of the Topopah Spring welded unit due to capillary-barrier effects above the vitric facies of the Calico Hill nonwelded unit. Within both facies of the Calico Hills nonwelded unit, a lateral component of flow occurs due to anisotropy. In the zeolitic facies, a larger component of vertical flow occurs due to the presence of a discontinuous fracture system. Flow along the faults is presumed to be vertical adjacent to the welded units. Where lateral flow occurs above the nonwelded units, perched water may be present adjacent to the fault.

Two aspects of this conceptual model are examined in the report. It is of interest to examine the dependence of predicted flow patterns on matrix-dominated versus fracture-dominated flow in the welded tuff units. Currently, no laboratory or field data are available to establish the conditions under which water in the unsaturated fractured rock flows through the rock matrix versus the fractures. However, the effects of matrix- versus fracture-dominated flow in the highly fractured, welded tuff units are investigated theoretically. Second, the conditions leading to lateral flow above the repository unit are investigated. The occurrence of lateral flow is important to establish because it may reduce the amount of water that can flow through the repository horizon.

4.0 NUMERICAL MODEL

The numerical model TOUGH (Transport Of Unsaturated Groundwater and Heat; Pruess, 1983) was used in this investigation. The simulator solves the mass balance equations for water (liquid and vapor) and air as well as the energy equation for a system containing water and air. The liquid water flux is estimated using Darcy's law, whereas the vapor flux also has a diffusive component. The heat flux consists of conduction and convection as well as the diffusive vapor flux. In the present investigation, the full range of capabilities included in TOUGH was not used; TOUGH was used to model the isothermal flow of liquid water for a system containing water and air. The primary variables used in the TOUGH simulator are pressure, temperature, and air mass fraction for elements in single-phase condition and pressure, gas saturation, and temperature for two-phase nodes. Water properties are calculated using equations given by the International Formulation Committee (1967); the ideal gas law is used to approximate the properties of air, and its solubility in the liquid phase is calculated using Henry's law. The numerical model uses the integral finite-difference method (Edwards, 1969; Narasimhan and Witherspoon, 1976) for formulating the governing equations and discretizing the flow region. The equations are solved simultaneously using Newton-Raphson iteration, and the linearized equations are solved using a direct matrix solver (Duff, 1977). The simulator TOUGH is a modified version of the geothermal simulator MULKOM which has been validated against many theoretical problems (Pruess, 1983).

5.0 THEORETICAL STUDIES

In the theoretical studies, transient simulations were carried out until the liquid saturation remained constant to within 1% throughout the flow region and steady-state conditions were said to be established. Infiltration rates were generally selected from the average annual range of net infiltration estimated by Montazer and Wilson (1984), since seasonal variations in surface flux are generally damped out within a few tens of meters of the ground surface. Infiltration was assumed to be temporally and spatially uniform along the ground surface.

5.1 One-Dimensional Flow Simulations

Simulations of steady-state, one-dimensional, vertical flow through the unsaturated zone at Yucca Mountain were performed in order to check that the numerical code produces results that are consistent with the input data and to make a preliminary comparison of the theoretical results with measured matric-potential and liquid-saturation data. This comparison focuses on the potential repository unit, the Topopah Spring welded unit. The discretized flow region, shown in Figure 12, is composed of layers of Tiva Canyon welded unit, Paintbrush nonwelded unit, Topopah Spring welded unit, and Calico Hills (vitric) nonwelded unit. The thickness of each unit corresponds approximately to the average thickness at the Yucca Mountain site. The water table forms the lower boundary condition, and a constant flux, or infiltration rate, is specified along the upper boundary. The material properties are listed in Table 2. Matrix-flow conditions were assumed for the welded units. This was done by assigning to the welded units the relatively low values of absolute permeability measured on matrix samples. In addition, the characteristic curves representing the Topopah Spring welded unit were derived from measurements made on matrix material. Similar data were not available for the matrix of the Tiva Canyon welded unit, so the theoretical fracture curves were used. Note that while values of porosity are assigned to the units, the steady-state solution is

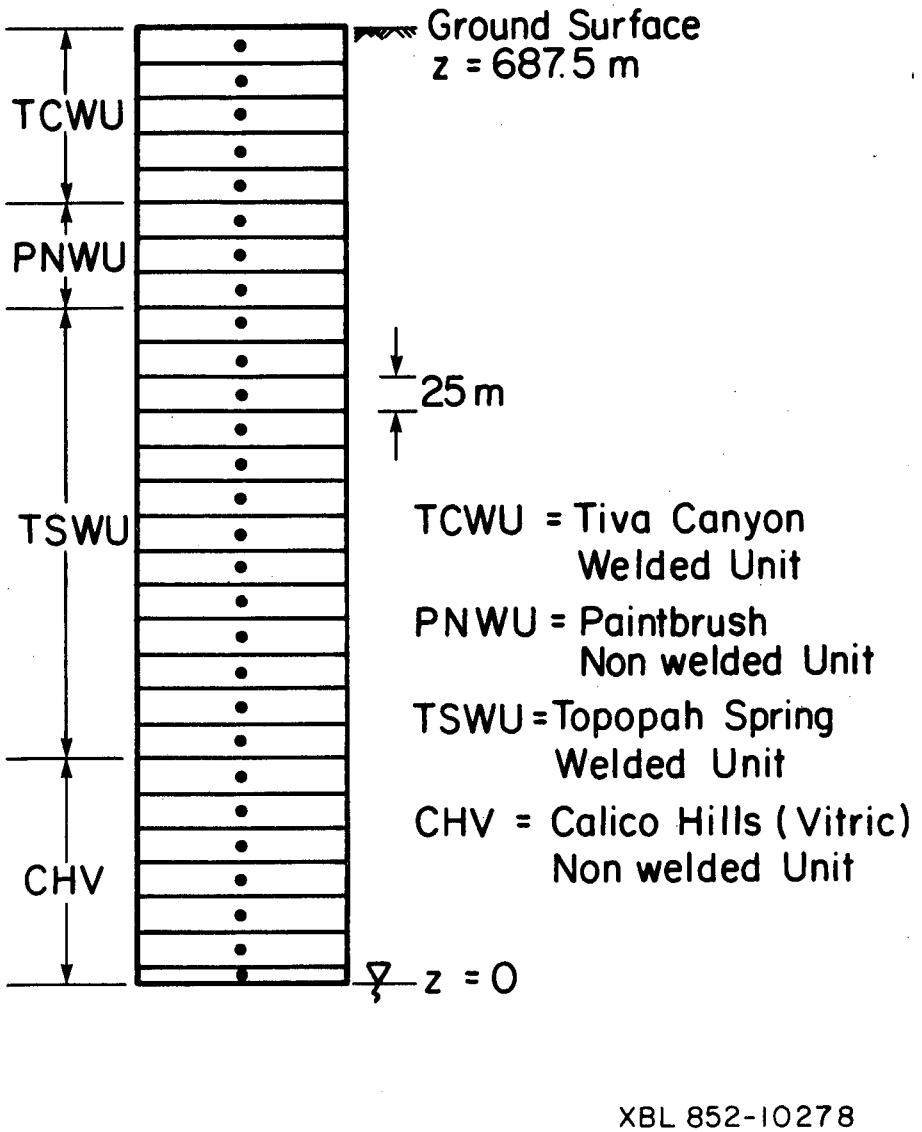

Figure 12. Discretized flow region for one-dimensional flow simulations.

Table 2. Material properties specified in the one-dimensional simulations.

Unit Name	Porosity	Absolute Vertical Permeability (m^2)	Equations for Characteristic Curves	van Genuchten Parameters*				
				$S_{r,l}$	$S_{s,l}$	α (bar^{-1})	n	m
Tiva Canyon welded unit	0.12	2.4×10^{-18}	$\phi_m = 1.34\ S_l^{-.491}$ $k_{r,l} = S_l^{1.936}$	-	-	-	-	-
Paintbrush nonwelded unit	0.46	1.0×10^{-15}	van Genuchten*	.166	.959	3.645	2.250	.5555
Topopah Spring welded unit	0.14	3.9×10^{-18}	van Genuchten*	.318	.984	1.147	3.040	.671
Calico Hills (vitric) nonwelded unit	0.37	5.0×10^{-16}	van Genuchten*	.31	1.0	1.37	2.345	.5735

*van Genuchten equations:

$$S_l\ (\ |\ \phi_m\ |\ ) = S_{r,l} + \frac{S_{s,l} - S_{r,l}}{\left[1 + (\alpha\ |\ \phi_m\ |\ )^n\right]^m}$$

$$k_{r,l}\ (\ |\ \phi_m\ |\ ) = \frac{\left\{1 - (\alpha\ |\ \phi_m\ |\ )^{n-1}\left[1 + (\alpha\ |\ \phi_m\ |\ )^n\right]^{-m}\right\}^2}{\left[1 + (\alpha\ |\ \phi_m\ |\ )^n\right]^{m/2}}$$

independent of the porosity that is assumed.

Four runs were made, each with a different infiltration rate: Q = 0.001, 0.01, 0.1, and 1.0 mm/yr. For all cases, static initial conditions were used; the matric potential at each node was initially specified as:

$$\phi_m = -\rho_l \, g z$$

where z is the distance from the nodal point to the water table. Note that for one-dimensional, vertical, isothermal flow of liquid water, static initial conditions are independent of the material properties assigned to the units.

Figure 13 shows the computed matric-potential profile at steady state for an infiltration rate of Q = 0.001 mm/yr and for static conditions, Q = 0. The matric potential for static conditions in the repository unit ranges from approximately -50 bars to -15 bars. In contrast, the in-situ measurements shown in Figure 8 indicate that the matric potential generally decreases with depth, ranging between -1 and -10 bars. The in-situ measurements, therefore, do not reflect a static, one-dimensional, isothermal flow system.

As shown in Figure 13, the numerical model predicts a constant matric potential of approximately -2.1 bars throughout most of the Topopah Spring welded unit for Q = 0.001 mm/yr. The reason for this is as follows. Given a homogeneous material, a flux less than the saturated hydraulic conductivity, and steady-state vertical flow conditions, then a "transmission zone" may form in which the matric potential and liquid saturation are constant and the corresponding hydraulic conductivity equals the magnitude of the flux. This is a well-known concept from soil physics (see, for example, Hillel, 1980) and it can be demonstrated in terms of Darcy's law. For the type of system outlined above, Darcy's law can be written as:

$$Q = \frac{k_{r,l}(S_l)\, k_a\, \rho_l\, g}{\mu_l} \left(\frac{\partial \phi_m}{\partial z} + 1 \right)$$

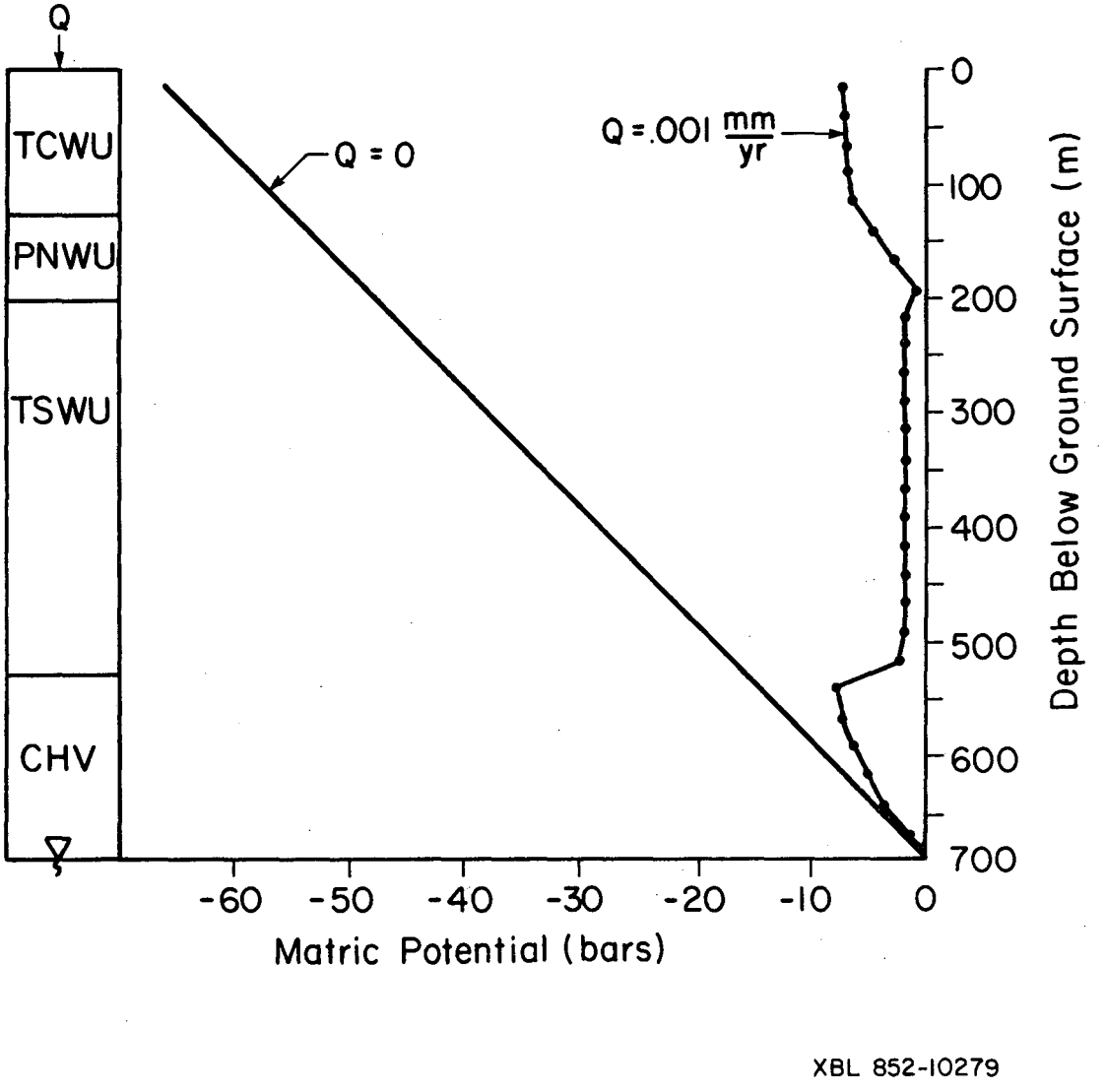

Figure 13. Profile of matric potential at steady state for the one-dimensional simulation in which Q = 0.001 mm/yr and for static conditions, Q = 0.

where Q is the flux, i.e., flow rate per unit cross-sectional area. In the transmission zone, ϕ_m is constant so that:

$$Q = \frac{k_{r,l}\ (S_l)\ k_a \rho_l\, g}{\mu_l} \tag{4}$$

Equation 4 states that the flux specified at the surface fixes the value of the relative permeability in the transmission zone. In turn, the relative permeability determines the values of liquid saturation and matric potential as specified by the characteristic curves. Therefore, in Figure 13, for Q = 0.001 mm/yr, the value of ϕ_m = -2.1 bars is determined by the relative permeability required to transmit a flux of 0.001 mm/yr through the Topopah Spring welded unit. Clearly, confidence in the results of the simulations cannot exceed confidence in the characteristic-curve data nor in the estimates of flux. The analysis also suggests that the values of the matric potential and the liquid saturation in the transmission zone can be computed by hand. The numerical code TOUGH was used here as an exercise to check that the code produces results that are consistent with the input data.

Figure 14 shows the matric-potential profiles at steady state for the four infiltration rates. As expected, the matric potential increases as the infiltration rate increases. The matric potential throughout most of the Topopah Spring welded unit is a constant value consistent with the applied flux and characteristic curves. None of the simulations produces the observed increase in matric potential with depth in the repository unit. With the exception of Q = 1.0 mm/yr, all of the simulations fall within the observed range of matric potential from borehole USW UZ-1 (-1 to -10 bars), indicating that the characteristic curves for the Topopah Spring welded unit are generally consistent with the field measurements for values of net infiltration that are less than 1.0 mm/yr.

Figure 15 shows the liquid saturation as a function of depth for static conditions and for the four infiltration rates. Measurements of liquid saturation in the Topopah Spring welded unit average approximately 0.65 and show a general increase with depth

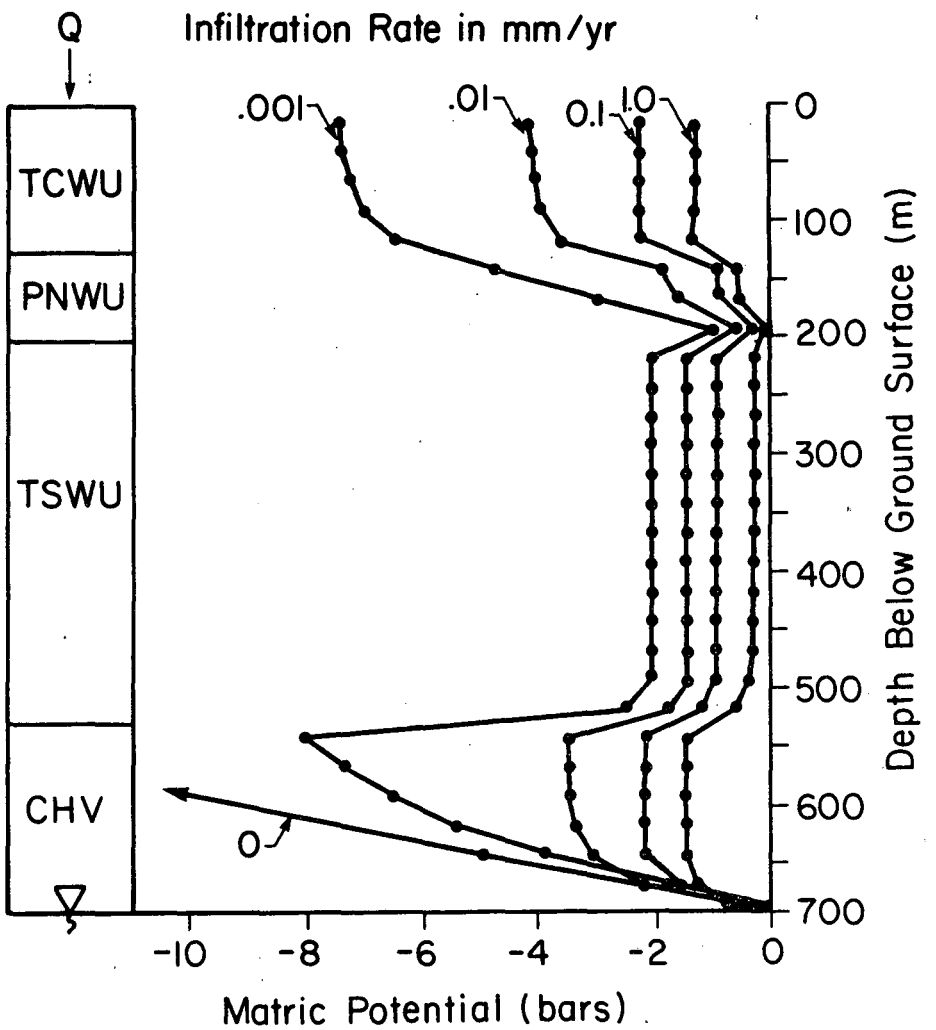

XBL 852-10280

Figure 14. Profiles of matric potential at steady state for one-dimensional simulations.

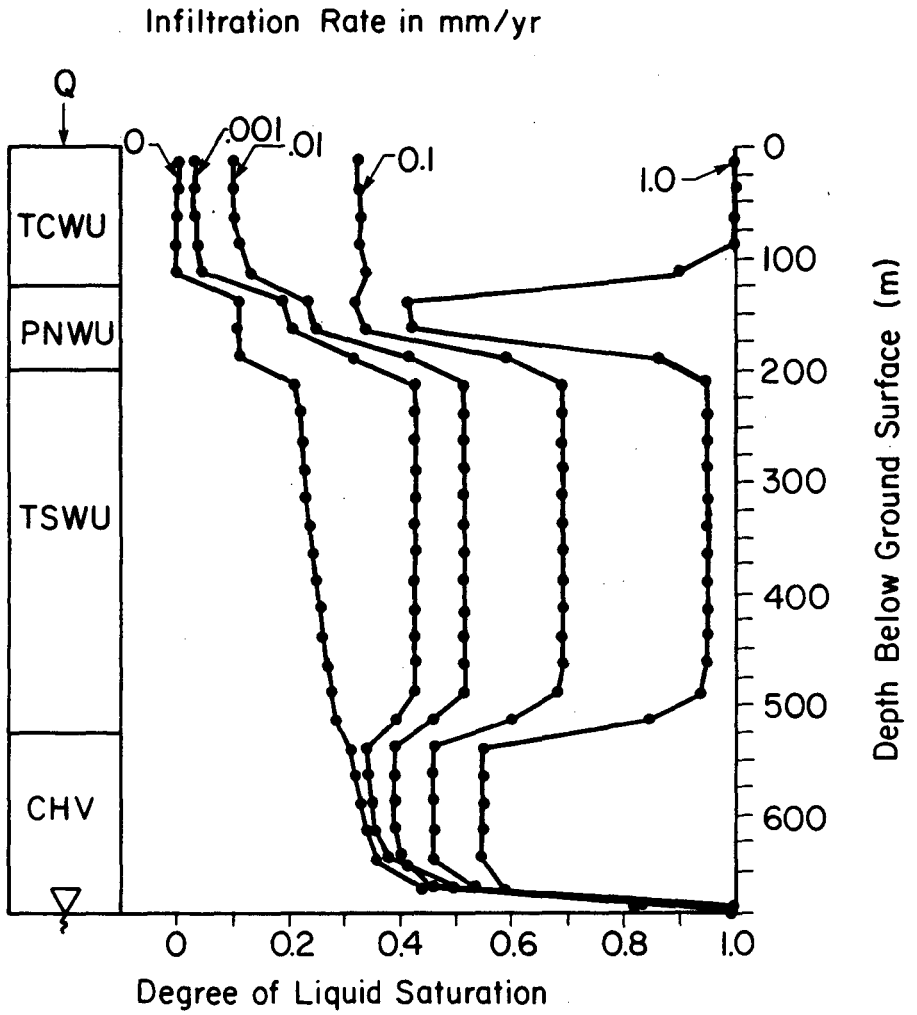

XBL 852-10281

Figure 15. Profiles of liquid saturation at steady state for one-dimensional simulations.

from 0.30 to 0.80. The predicted results are uniform with depth in the repository unit and therefore do not support the observed increase in liquid saturation with depth. The simulation in which the infiltration rate equals 0.1 mm/yr agrees best with the measured average value of 0.65.

5.2 Two-Dimensional Flow Simulations

A series of two-dimensional flow simulations were designed to: (a) investigate the general flow patterns predicted on the basis of the available data, (b) compare theoretical predictions with measured profiles of matric potential and liquid saturation, and (c) test some of the concepts proposed in the conceptual model.

The discretized, two-dimensional flow region is shown in Figure 16. In keeping with the preliminary nature of the investigation, the mesh is coarse; it contains 208 elements, each measuring 125 m by 25 m. The region is bounded below by the water table and above by the ground surface. The two vertical boundaries are impermeable; one corresponds to the western flank of Yucca Mountain and the other corresponds to the eastern extent of the Fault Zone. Initial conditions are static unless otherwise noted; however, the steady-state solution of the nonlinear equation governing fluid flow in this system is not unique and may depend on the choice of initial conditions.

The results of four sets of simulations are presented. First are the matrix-flow simulations in which flow through the welded units is assumed to be controlled by the properties of the rock matrix. Second are the fracture-flow simulations in which flow is assumed to occur within the fractures of the welded units. Third are the fracture-matrix flow simulations in which flow through the welded units occurs as a combination of fracture and matrix flow. Fourth are a set of sensitivity studies that examine the effects of: (a) changing the permeability of the Fault Zone, (b) adding a second fault zone along the western boundary of the flow region, and (c) reducing the size of the elements by a factor of two.

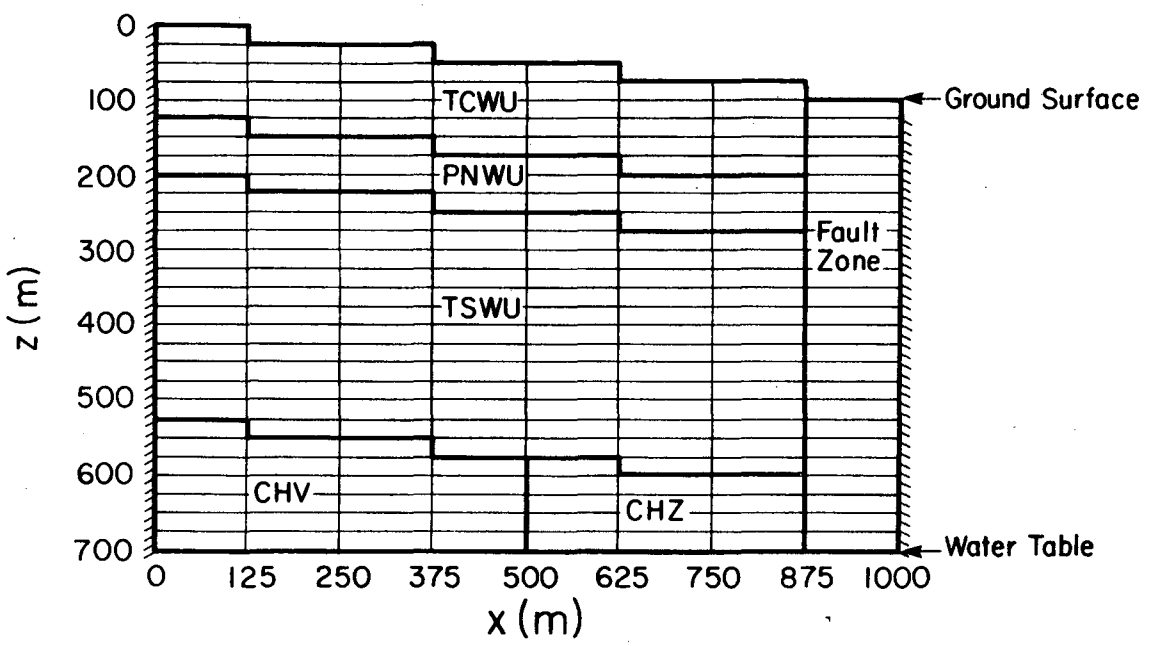

TCWU = Tiva Canyon Welded Unit
PNWU = Paintbrush Nonwelded Unit
TSWU = Topopah Spring Welded Unit
CHV = Vitric Facies of Calico Hills Nonwelded Unit
CHZ = Zeolitzed Facies of Calico Hills Nonwelded Unit

XBL 852-10282

Figure 16. Discretized flow region used in the two-dimensional flow simulations.

5.2.1 Matrix-Flow Simulations

As in the one-dimensional studies, matrix-flow conditions in the welded units were simulated by assigning the Tiva Canyon and Topopah Spring welded units absolute permeabilities measured on samples of matrix material. A summary of all material properties specified in the matrix-flow simulations is given in Table 3. Note that the properties of the units that appeared in the one-dimensional simulations remain unchanged.

Two runs were made to investigate matrix-flow conditions. For Matrix-Flow Simulation #1 (MX1), an infiltration rate of 0.015 mm/yr was specified along the ground surface; for Matrix-Flow Simulation #2 (MX2), the infiltration rate was increased to 1.0 mm/yr. The steady-state solution from MX1 was used as the initial conditions for MX2. Figure 17 shows a vector plot of the mass flux through the flow system at steady state for MX1. The corresponding plot for MX2 is qualitatively similar and, therefore, is not shown. In both simulations, lateral flow occurs within the Paintbrush nonwelded unit and, to a smaller degree, in portions of the Tiva Canyon welded unit adjacent to the Fault Zone. Table 4 provides a comparison of the two runs in terms of proportions of lateral flow and flux through the repository unit. The lateral flow is normalized against the total amount of infiltration that enters along the surface of the Tiva Canyon welded unit. In this way, water that directly enters the Fault Zone at the ground surface is not considered to be part of the lateral flow. Table 4 shows that the percentage of the flow diverted laterally into the Fault Zone decreases from 57% to 48% as the infiltration rate increases from 0.015 mm/yr to 1.0 mm/yr. This is due to decreased resistance to flow (higher liquid permeabilities) in the Topopah Spring welded unit for higher infiltration rates. As a result of lateral flow, the Fault Zone transmits most of the total flow through the system at steady state and the flux through the repository unit is reduced. The average flux through the repository unit scales approximately with the infiltration rate, i.e., as the infiltration rate is reduced from 1.0 mm/yr to 0.015 mm/yr, the flux is reduced by a similar factor from 4.5×10^{-1} mm/yr to 5.3×10^{-3} mm/yr.

Table 3. Material properties specified in the matrix-flow simulations.

Unit Name	Porosity	Absolute Vertical Permeability (m^2)	Anisotropy Ratio (Horizontal/ Vertical)	Equations for Characteristic Curves	van Genuchten Parameters*				
					$S_{r,l}$	$S_{s,l}$	α (bar^{-1})	n	m
Tiva Canyon welded unit	0.12	2.4×10^{-18}	1	$\phi_m = -1.34\ S_l^{-.491}$ $k_{r,l} = S_l^{1.936}$	-	-	-	-	-
Paintbrush nonwelded unit	0.46	1.0×10^{-15}	10	van Genuchten*	.166	.959	3.645	2.250	.5555
Topopah Spring welded unit	0.14	3.9×10^{-18}	1	van Genuchten*	.318	.984	1.147	3.040	.671
Calico Hills (vitric) nonwelded unit	0.37	5.0×10^{-16}	10	van Genuchten*	.31	1.0	1.37	2.345	.5735
Calico Hills (zeolitic) nonwelded unit	0.33	9.3×10^{-18}	1	input as table of values (see Figures 3d & 5d)	-	-	-	-	-
Fault Zone	0.05	5×10^{-11}	0.02	$\phi_m = -0.1\ S_l^{-.497}$ $k_{r,l} = S_l^{1.945}$	-	-	-	-	-

*van Genuchten equations:

$$S_l\ (\ |\ \phi_m\ |\ ) = S_{r,l} + \frac{S_{s,l} - S_{r,l}}{\left[1 + (\alpha\ |\ \phi_m\ |\ )^n\right]^m}$$

$$k_{r,l}\ (\ |\ \phi_m\ |\ ) = \frac{\left\{1 - (\alpha\ |\ \phi_m\ |\ )^{n-1}\left[1 + (\alpha\ |\ \phi_m\ |\ )^n\right]^{-m}\right\}^2}{\left[1 + (\alpha\ |\ \phi_m\ |\ )^n\right]^{m/2}}$$

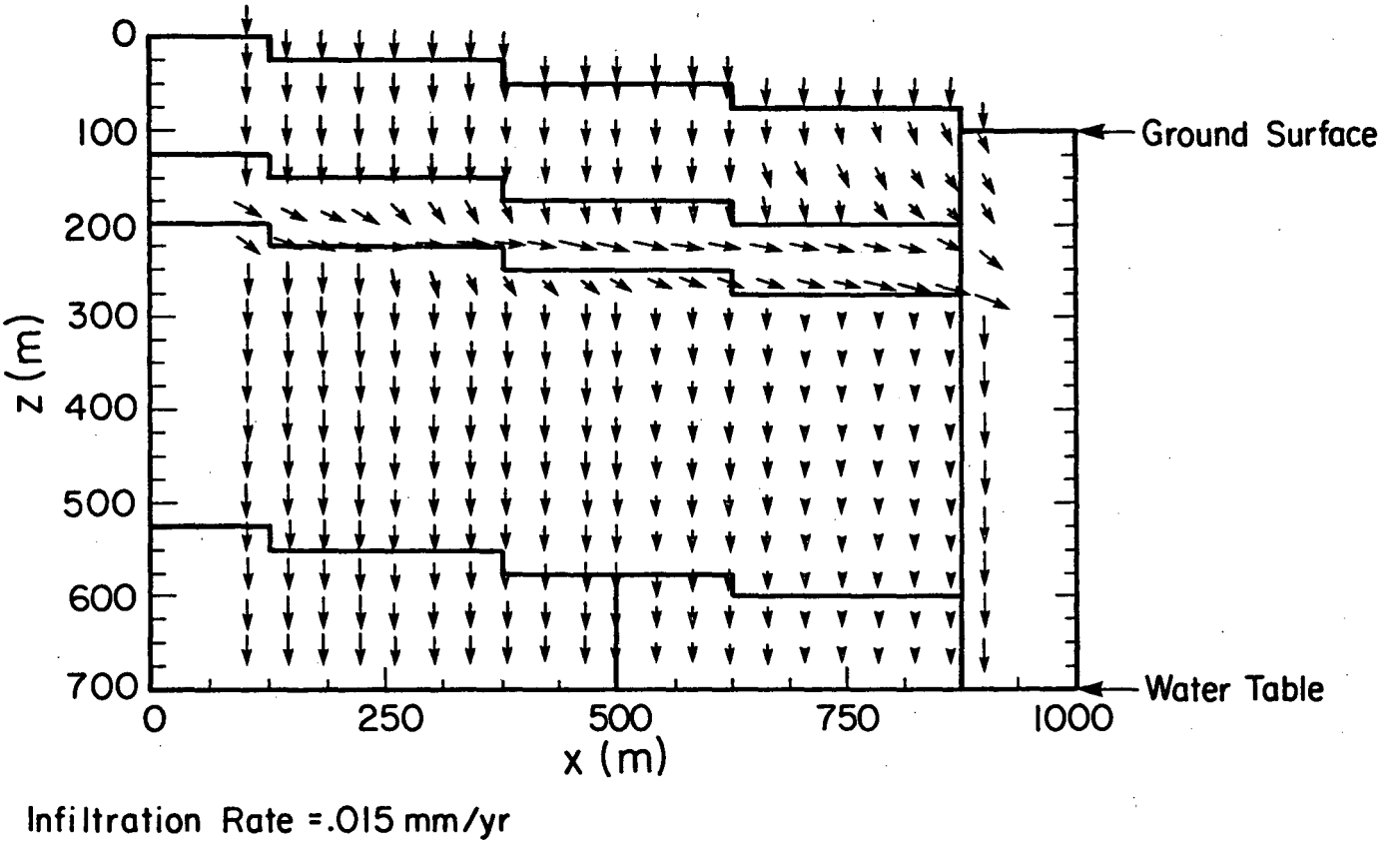

Figure 17. Vector plot of computed mass flux through the flow system at steady state for Matrix-Flow Simulation #1.

Table 4. Comparison of lateral flow and flux through the repository unit for the matrix-flow simulations.

	Matrix-Flow Simulation #1	Matrix-Flow Simulation #2
Infiltration Rate (mm/yr)	0.015	1.0
Percentage of flow diverted laterally into Fault Zone above TSWU*	57%	48%
Average flux through TSWU* (mm/yr)	5.3×10^{-3}	4.5×10^{-1}

*TSWU = Topopah Spring Welded Unit

Figure 18 and 19 are contour diagrams of the computed matric-potential distribution at steady state for MX1 and MX2, respectively. The matric potential is generally lower for the case with the lower infiltration rate. For example, in MX1, the matric potential varys between -2 bars and -4 bars within the Topopah Spring welded unit; in MX2, it is greater than -2 bars. As noted earlier, the observed decrease in matric potential in the repository unit is accompanied by a decrease in relative permeability and consequently, a greater percentage of the total flow is diverted laterally within the overlying unit in MX1 compared with MX2 (see Table 4).

Figures 20 and 21 are contour diagrams of the computed liquid-saturation distribution at steady state for MX1 and MX2, respectively. Overall, liquid saturations are higher for MX2 due to the higher infiltration rate. In the repository unit, liquid saturation varies between 0.35 and 0.50 for MX1 and between 0.50 and 0.95 for MX2.

Figure 22 shows the outflow across the water table as a function of time for MX1. The outflow at any given time is expressed as the percentage of the total inflow along the ground surface. The solid line in Figure 22 represents outflow along the entire length of the water table, whereas the dashed line represents outflow from the Fault Zone alone. Figure 22 demonstrates a feature common to all of the simulations, namely, that at early times, all of the outflow occurs across the base of the Fault Zone due to its relatively high permeability; water that passes through the repository unit arrives much later. It also appears from Figure 22 that steady-state conditions are reached after seven million years. Figure 22 is of interest only from a computational point of view since the time scale represents the simulated time from static initial conditions. While the ambient conditions at Yucca Mountain are unknown, it is doubtful that they are static. Therefore, the absolute arrival times and the time required to reach steady state are more directly related to the use of static initial conditions and should not be interpreted as an indication of the hydrologic response time of the present-day system to a given set of conditions.

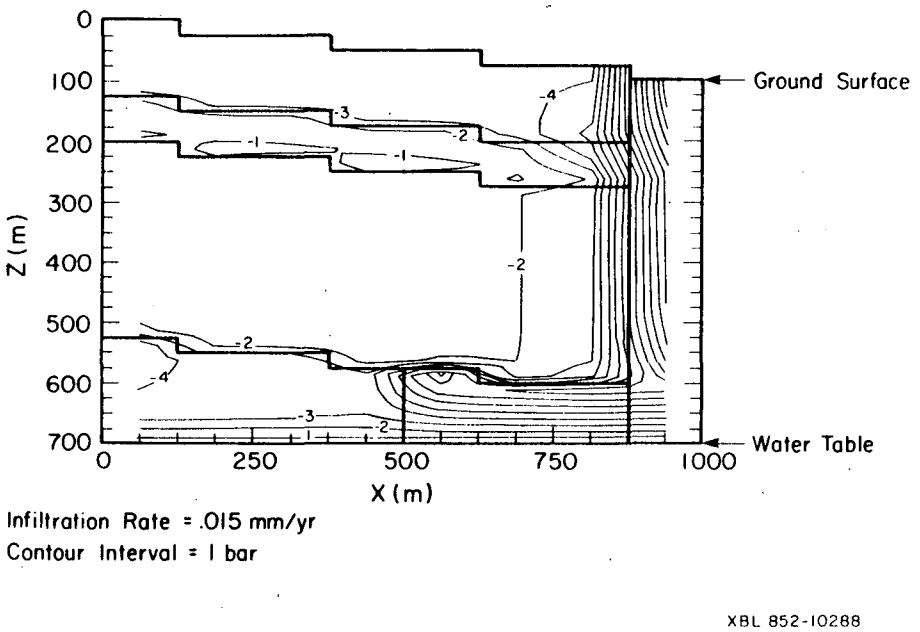

Figure 18. Contour diagram of the computed matric-potential distribution at steady state for Matric-Flow Simulation #1.

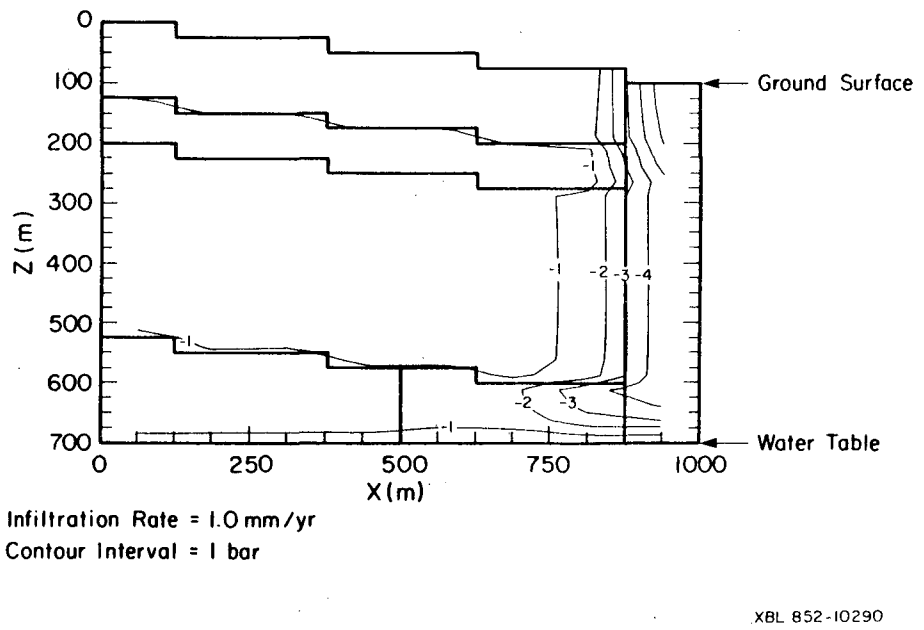

Figure 19. Contour diagram of the computed matric-potential distribution at steady state for Matrix-Flow Simulation #2.

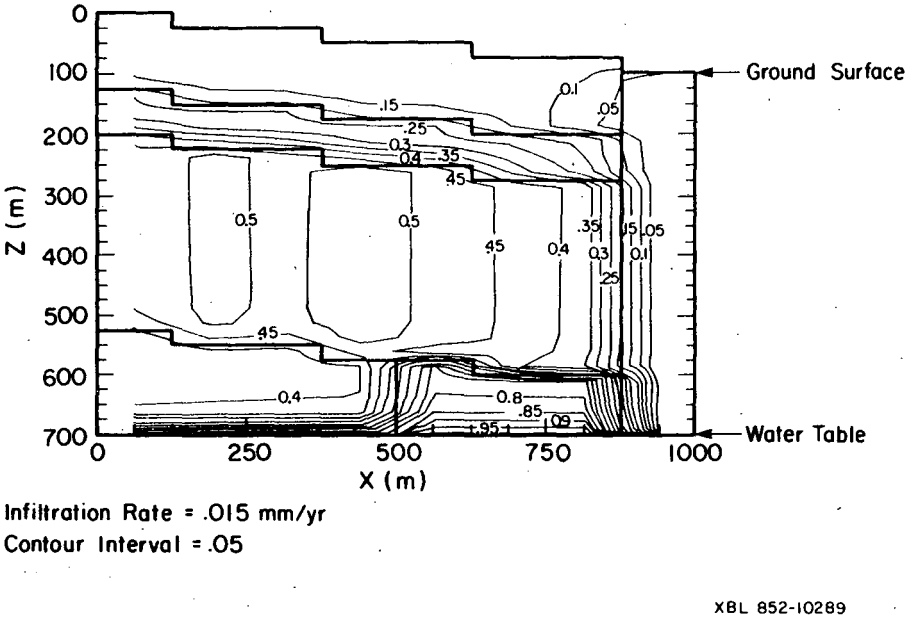

Figure 20. Contour diagram of the computed liquid-saturation distribution at steady state for Matrix-Flow Simulation #2.

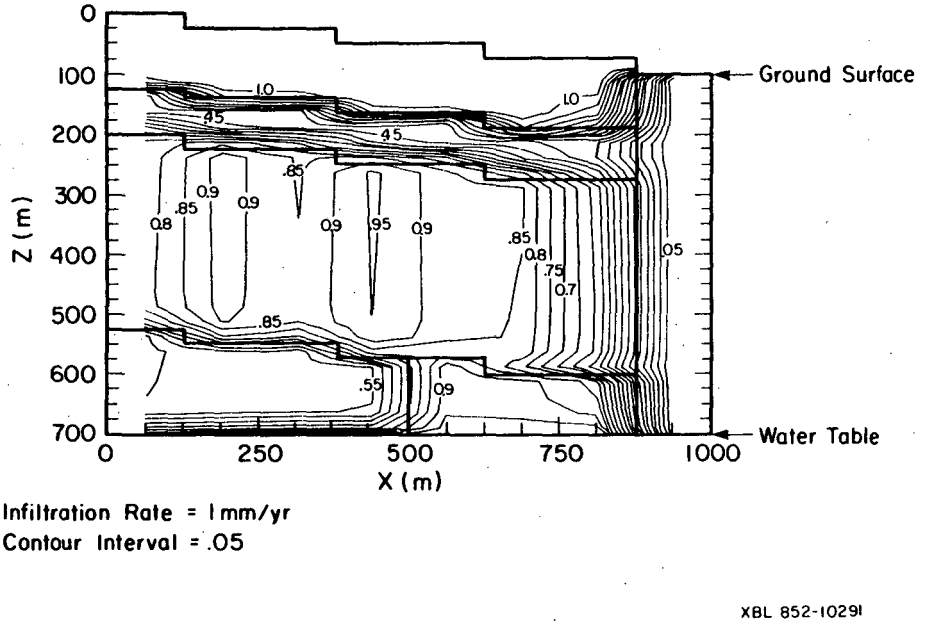

Figure 21. Contour diagram of the computed liquid-saturation distribution at steady state for Matrix-Flow Simulation #2.

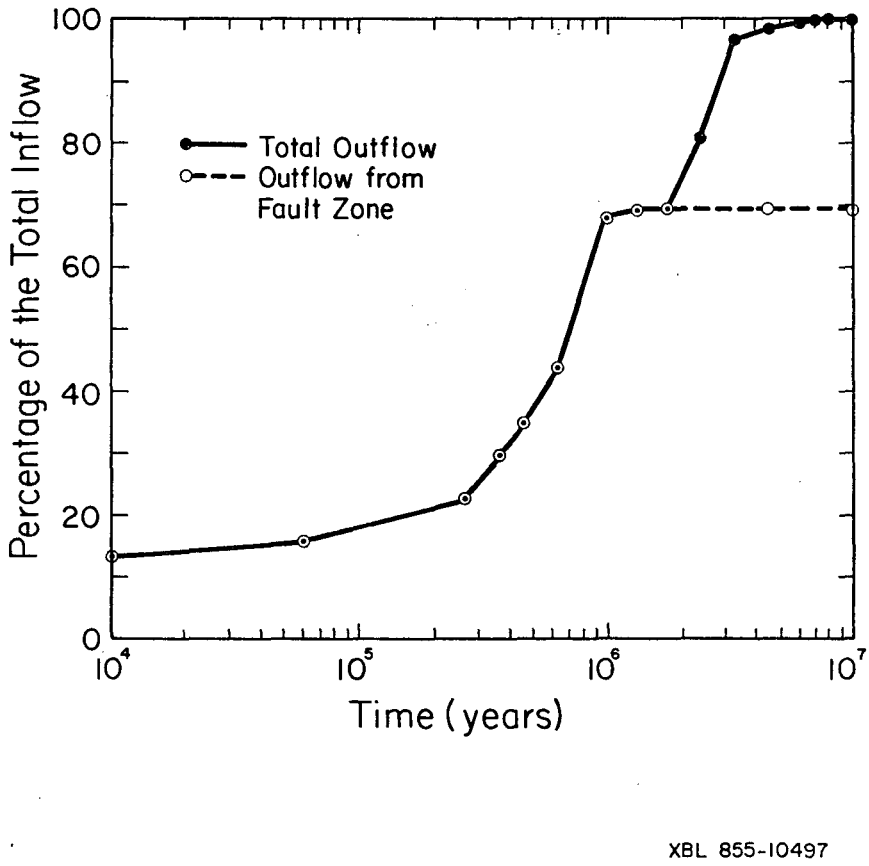

Figure 22. Outflow across the water table as a function of time for Matrix-Flow Simulation #1.

5.2.2 Fracture-Flow Simulations

In this study, fracture flow in unsaturated media is modeled in an implicit fashion. Theoretical characteristic curves thought to incorporate the physics of unsaturated flow through fractured rocks are used in conjunction with relatively high absolute bulk permeabilities representative of fractured tuff. Evaluation of the validity of this approach must await laboratory or field testing; however, at present it is considered a reasonable theoretical approach.

In the simulations presented in this section, the absolute permeability of the Tiva Canyon welded unit and the Topopah Spring welded unit were set equal and increased from the value in the matrix simulations of approximately $10^{-18}m^2$ to $10^{-14}m^2$. The higher value is representative of fractured tuff based on air-permeability tests at the Nevada Test Site (Montazer et al., 1985). The fracture-flow simulations are differentiated on the basis of the type of characteristic curves used to represent the Topopah Spring welded unit and the infiltration rate.

In the fracture-flow simulations, the Topopah Spring welded unit was assigned the same fracture characteristic curves used to represent the Tiva Canyon welded unit in the marix-flow simulations (see Figure 6). All material properties used for the fracture-flow simulations are given in Table 5. In Fracture-Flow Simulation #1 (FX1), an infiltration rate of 4.5 mm/yr was specified along the ground surface; in Fracture-Flow Simulation #2 (FX2), the infiltration rate was reduced to 1.0 mm/yr.

The vector plot of flux through the system at steady state for FX1 is shown in Figure 23 and is qualitatively similar to the corresponding plot for FX2. In contrast to the matrix-flow simulations, lateral flow occurs primarily at the base of both welded units, because the nonwelded units are less permeable than the welded units in the fracture-flow simulations. Table 6 provides a comparison of the two runs in terms of proportions of lateral flow and the average flux through the repository unit. In FX1, most of the lateral flow occurs at the base of the Topopah Spring welded unit and, therefore, a

Table 5. Material properties specified in the fracture-flow simulations.

Unit Name	Porosity	Absolute Vertical Permeability (m^2)	Anisotropy Ratio (Horizontal/ Vertical)	Equations for Characteristic Curves	van Genuchten Parameters*				
					$S_{r,l}$	$S_{s,l}$	α (bar^{-1})	n	m
Tiva Canyon welded unit	0.12	1.0×10^{-14}	1	$\phi_m = -1.34\ S_l^{-.491}$ $k_{r,l} = S_l^{1.936}$	-	-	-	-	-
Paintbrush nonwelded unit	0.46	1.0×10^{-15}	10	van Genuchten*	.166	.959	3.645	2.250	.5555
Topopah Spring welded unit	0.14	1.0×10^{-14}	1	$\phi_m = -1.34\ S_l^{-.491}$ $k_{r,l} = S_l^{1.936}$	-	-	-	-	-
Calico Hills (vitric) nonwelded unit	0.37	5.0×10^{-16}	10	van Genuchten*	.31	1.0	1.37	2.345	.5735
Calico Hills (zeolitic) nonwelded unit	0.33	9.3×10^{-18}	1	input as table of values (see Figures 3d & 5d)	-	-	-	-	-
Fault Zone	0.05	5×10^{-11}	0.02	$\phi_m = -0.1\ S_l^{-.497}$ $k_{r,l} = S_l^{1.945}$	-	-	-	-	-

*van Genuchten equations:

$$S_l\ (\ |\ \phi_m\ |\ ) = S_{r,l} + \frac{S_{s,l} - S_{r,l}}{\left[1 + (\alpha\ |\ \phi_m\ |\ )^n\right]^m}$$

$$k_{r,l}\ (\ |\ \phi_m\ |\ ) = \frac{\left\{1 - (\alpha\ |\ \phi_m\ |\ )^{n-1}\left[1 + (\alpha\ |\ \phi_m\ |\ )^n\right]^{-m}\right\}^2}{\left[1 + (\alpha\ |\ \phi_m\ |\ )^n\right]^{m/2}}$$

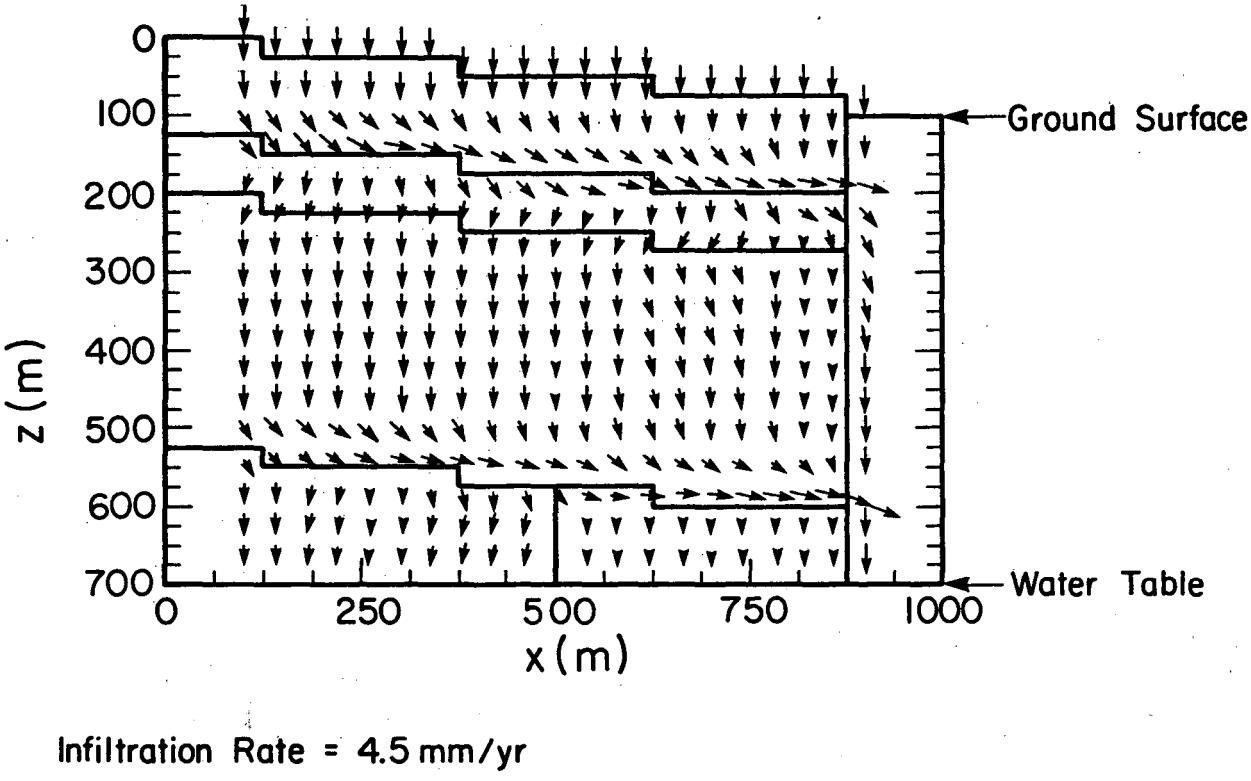

Figure 23. Vector plot of computed mass flux through the flow system at steady state for Fracture-Flow Simulation #1.

Table 6. Comparison of computed, steady-state lateral flow and flux through the repository unit for the fracture-flow simulations.

	Fracture-Flow Simulation #1	Fracture-Flow Simulation #2
Infiltration Rate (mm/yr)	4.5	1.0
Percentage of flow diverted laterally into Fault Zone		
a) above TSWU*	19	39
b) below TSWU*	25	25
Average flux through TSWU* (mm/yr)	3.5	0.53

*TSWU = Topopah Spring welded unit.

relatively high proportion of the infiltration passes through the unit. In FX2, the lower flux is accompanied by an increase in lateral flow above the Topopah Spring welded unit and, hence, the flux through the unit is reduced significantly.

Figures 24 and 25 are contour diagrams of the computed matric-potential distribution at steady state for FX1 and FX2, respectively. The matric potential is generally lower in FX2 because of the reduced infiltration. Figures 26 and 27 show diagrams for liquid saturation for FX1 and FX2, respectively. Saturations are low, less than 0.10, in the welded units and Fault Zone since these represent fracture saturations. However, it is possible to estimate the liquid saturation in the matrix of the Topopah Spring welded unit. Discrete fracture studies by Bodvarsson and Rulon (1985) show that for fracture spacing on the order of one meter or less, the matric potential in the fracture and matrix are equal at steady state. The liquid saturation in the matrix can be obtained from the corresponding moisture-retention curve, given the matric potential at steady state. Therefore, based on the computed steady-state matric potential and the moisture-retention curve for the Topopah Spring welded unit (Figure 3b), the liquid saturation in the matrix varies between 0.32 and 0.35 for FX1 and between 0.29 and 0.35 for FX2.

5.2.3 Fracture-Matrix Flow Simulations

In the fracture-matrix flow simulations, the relationship between relative permeability and matric potential was modified for the welded units. Figure 28 shows three curves that related, in a qualitative sense, permeabilty to matric potential and liquid saturation. This figure was modified from one in Montazer and Wilson (1984, Figure 6). The curves are intended to represent drainage of fractured porous medium in which the matrix has very low permeability. The matrix curve is hypothetical, the fracture curve was developed using a fracture model, and the "combined curve" is assumed to represent the combined behavior of flow through the fracture and flow through the matrix. At high liquid saturations and large values of matric potential, the permeability of the

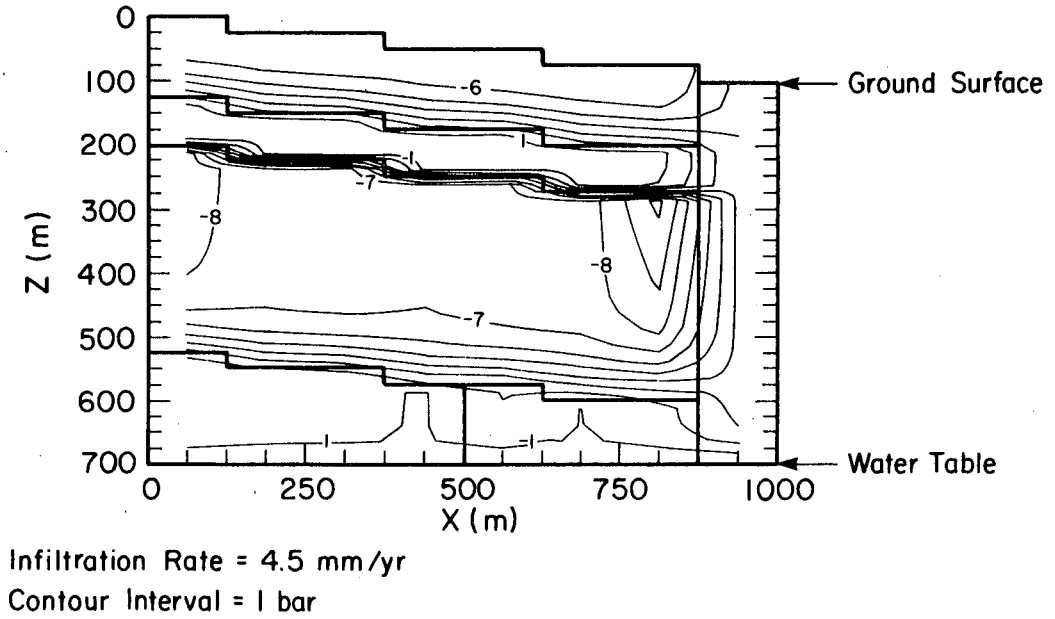

Figure 24. Contour diagram of the computed matric-potential distribution at steady state for Fracture-Flow Simulation #1.

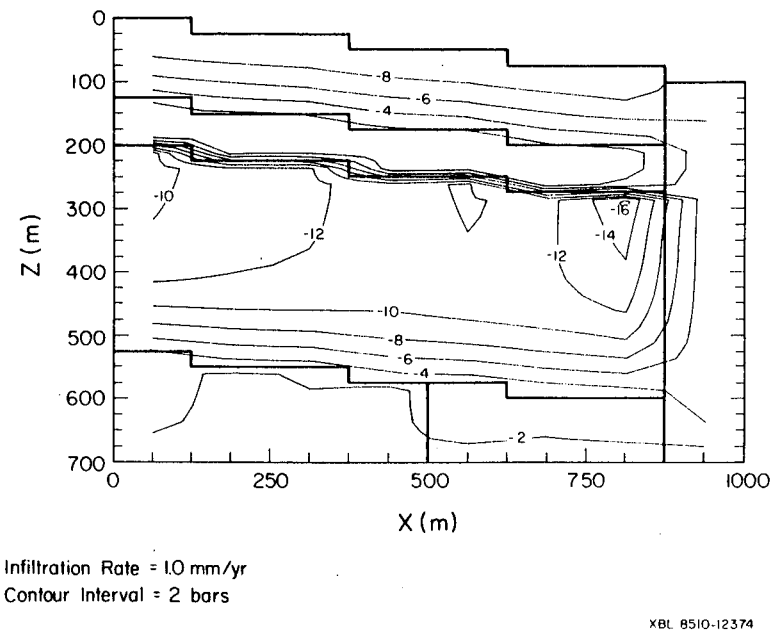

Figure 25. Contour diagram of the computed matric-potential distribution at steady state for Fracture-Flow Simulation #2.

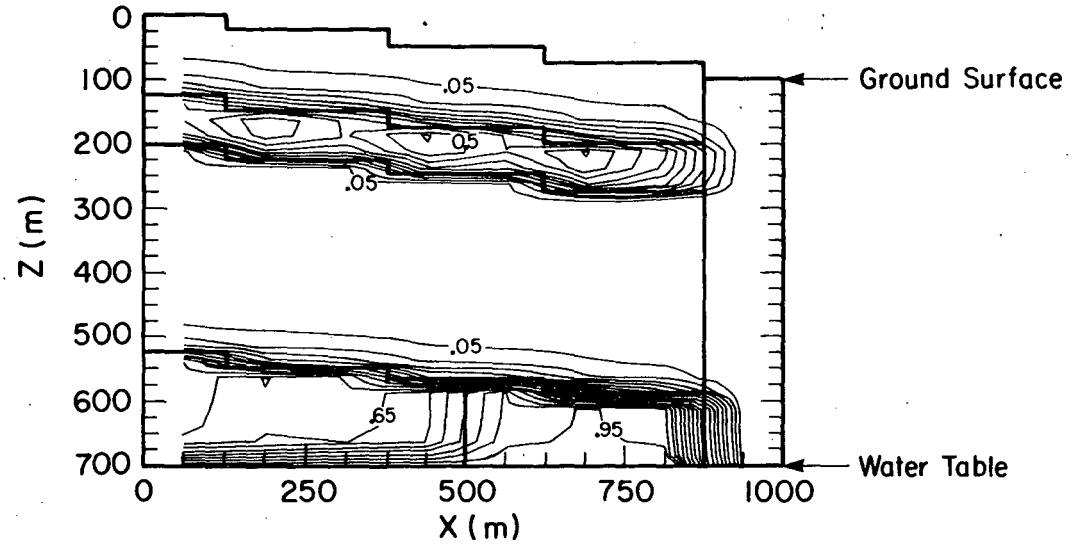

Infiltration Rate = 4.5 mm/yr
Contour Interval = .05

XBL 852-10293

Figure 26. Contour diagram of the computed liquid-saturation distribution at steady state for Fracture-Flow Simulation #1.

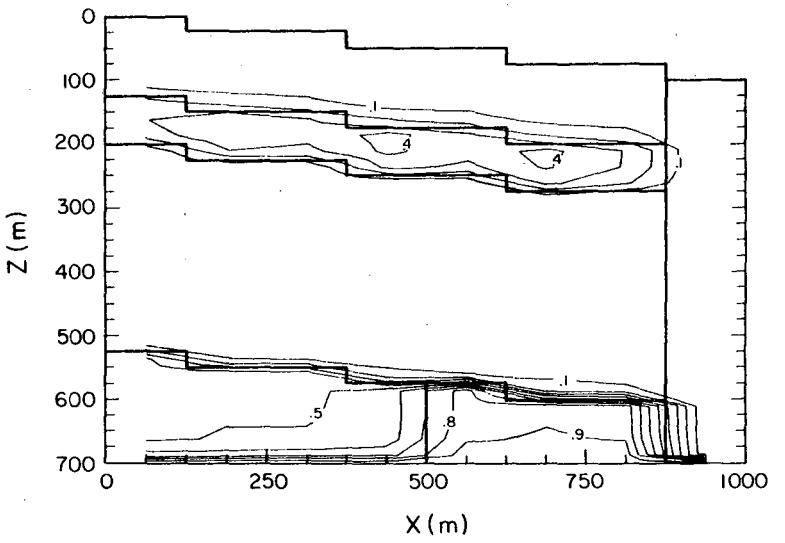

Infiltration Rate = 1.0 mm/yr
Contour Interval = 0.1

XBL 8510-12355

Figure 27. Contour diagram of the computed liquid-saturation distribution at steady state for Fracture-Flow Simulation #2.

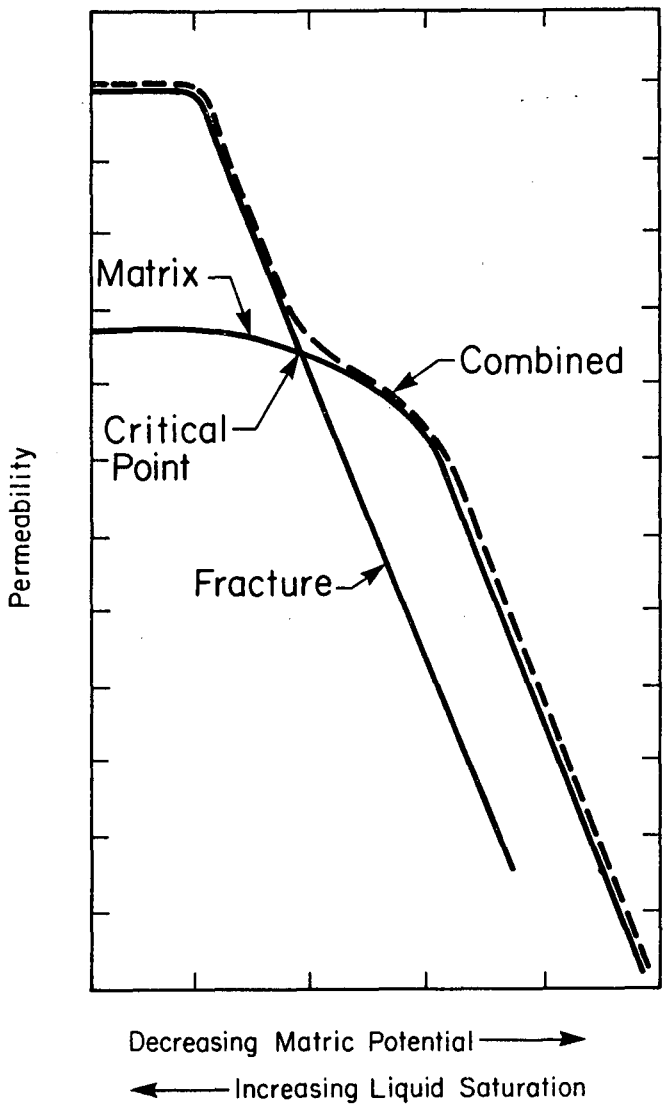

Figure 28. Qualitative representation of the relationship between permeability, matric potential, and liquid saturation for a "combined" fracture-matrix medium (modified from Montazer and Wilson, 1984, Figure 6).

fractures is much higher than that of the matrix and therefore dominates the behavior of the system. The combined curve follows the fracture curve in this region. As the matric potential and liquid saturation decrease, flow through the matrix becomes increasingly significant until the critical point is reached and fracture flow is equal to matrix flow for a given hydraulic gradient. Beyond the critical point, flow through the fracture is insignificant compared with matrix flow so the combined curve follows the matrix curve.

For Fracture-Matrix Flow Simulation #1 (FXMX1), the hypothetical combined curve shown in Figure 29 was used to represent the Tiva Canyon and Topopah Spring welded units. This curve was chosen because the fracture curve is similar to the curves used in FX1; in particular, the air-entry value is -1.34 bars. The critical point occurs at a matric potential of approximately -10 bars. All other material properties listed in Table 5 remained unchanged. For FXMX1, an infiltration rate of 4.5 mm/yr was used.

The results of FXMX1 did not differ significantly from the results of FX1. Figure 30 shows the computed matric-potential distribution at steady state for FXMX1. The matric potential in the Topopah Spring welded unit generally remains above the critical point of the combined, relative-permeablity curve so that conditions correspond to a dominance of fracture flow. This accounts for the similarities between FX1 and FXMX1. The distribution of computed liquid saturation and the amount and location of lateral flow for FXMX1 essentially remained unchanged from FX1.

In Fracture-Matrix Flow Simulation #2 (FXMX2), the combined curve shown in Figure 31 was used to represent the welded units. This curve is taken directly from Montazer and Wilson (1984, Figure 6) and differs from the previous combined curve in that it is shifted two orders of magnitude along the horizontal axis. The air-entry value is now -0.0134 bar rather than -1.34 bars and the critical point occurs at a matric potential value of -0.1 bar. By increasing the air-entry value two orders of magnitude, the effective aperture is increased from 0.3 μm to 30 μm. All other aspects of the problem remain unchanged and the infiltration rate was specified as 4.5 mm/yr.

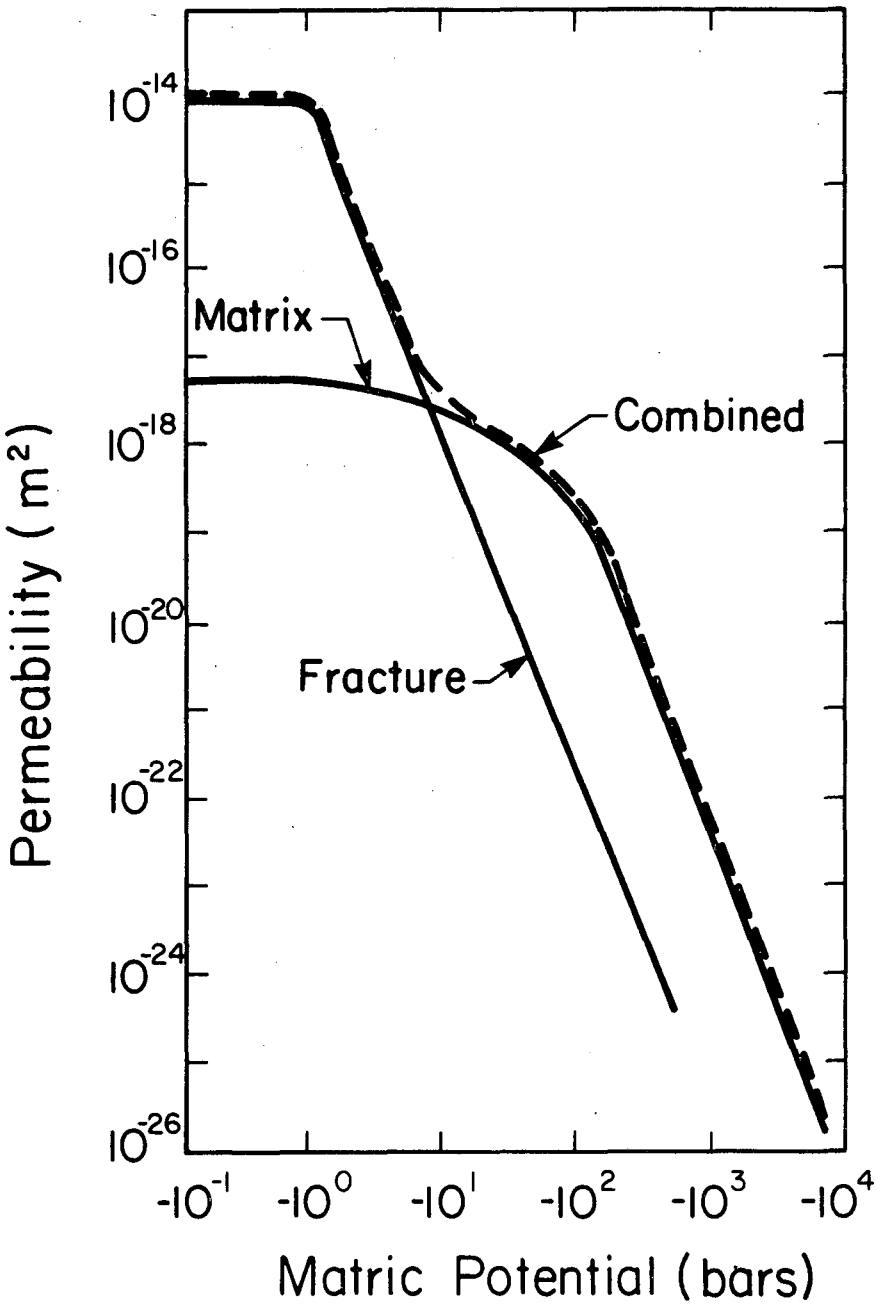

Figure 29. Hypothetical combined curve used in Fracture-Matrix Flow Simulation #1 (modified from Montazer and Wilson, 1984, Figure 6).

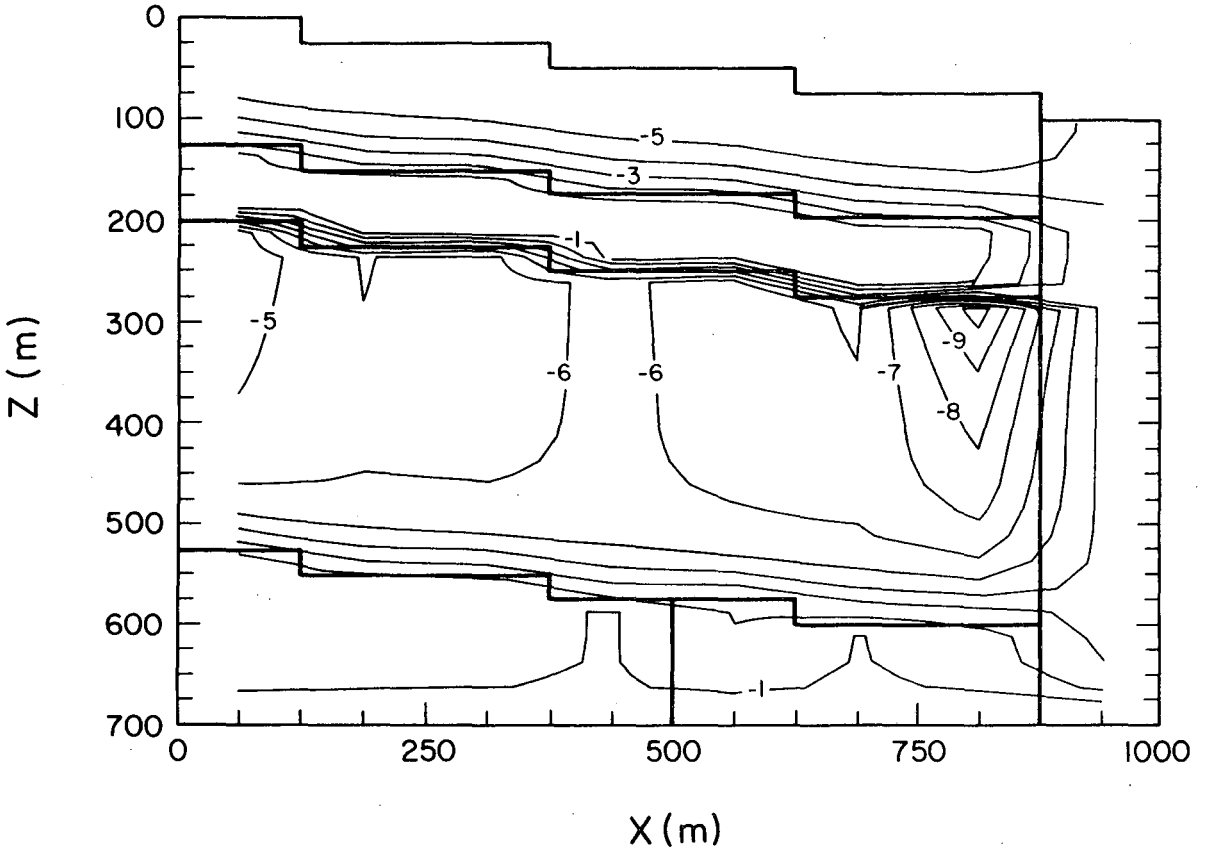

Infiltration Rate = 4.5 mm/yr
Contour Interval = 1 bar

XBL 8510-12349

Figure 30. Contour diagram of the computed matric-potential distribution at steady state for Fracture-Matrix Flow Simulation #1.

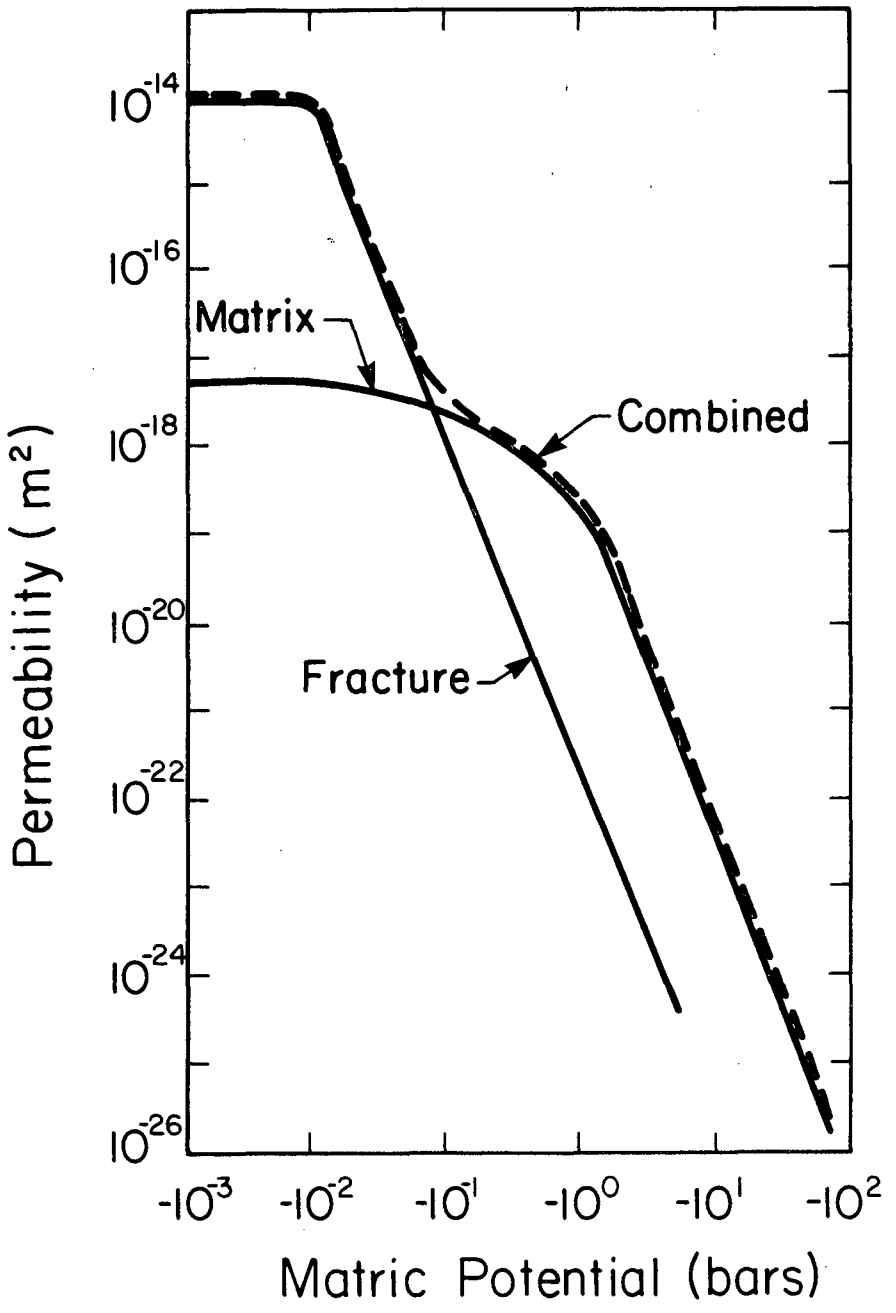

Figure 31. Combined curve used in Fracture-Matrix Flow Simulation #2 (Montazer and Wilson, 1984, Figure 6).

A vector plot of the mass flux at steady state for FXMX2 is shown in Figure 32. Flow is vertical throughout most of the system and, compared to the previous fracture- and fracture-matrix flow simulations, less lateral flow enters the Fault Zone. Thirteen percent of the flow above the Topopah Spring welded unit is diverted laterally into the Fault Zone above the unit and five percent is diverted at the base. The average flux through the repository unit is 3.8 mm/yr.

Figure 33 shows a contour diagram of the computed matric-potential distribution at steady state for FXMX2. Matric potential within the entire system is greater than -5 bars; in the repository unit the matric potential is, on the average, approximately -0.05 bar. The permeability in the Topopah Spring welded unit is, therefore, relatively high and the proportion of lateral flow above the unit is relatively small. Since the matric potential is greater than the critical value in the Topopah Spring welded unit, this simulation corresponds to a dominance of fracture flow. In addition, note that the matric-potential gradient is negligible throughout most of the flow system, resulting in dominantly vertical flowpaths driven by the gravity-potential gradient.

Figure 34 shows a contour diagram of liquid saturation for FXMX2. It is similar to the earlier simulations and indicates that the liquid saturation in the fractures is less than 0.1 in the welded units. Based on an average matric potential in the Topopah Spring welded unit of -0.05 bar, the liquid saturation of the matrix is approximately 0.98.

5.2.4 Sensitivity Studies

Studies were performed to test the sensitivity of the results to the Fault Zone properties, the presence of a second fault zone along the western boundary of the flow region, and the size of the elements. These simulations can be viewed as a subset of

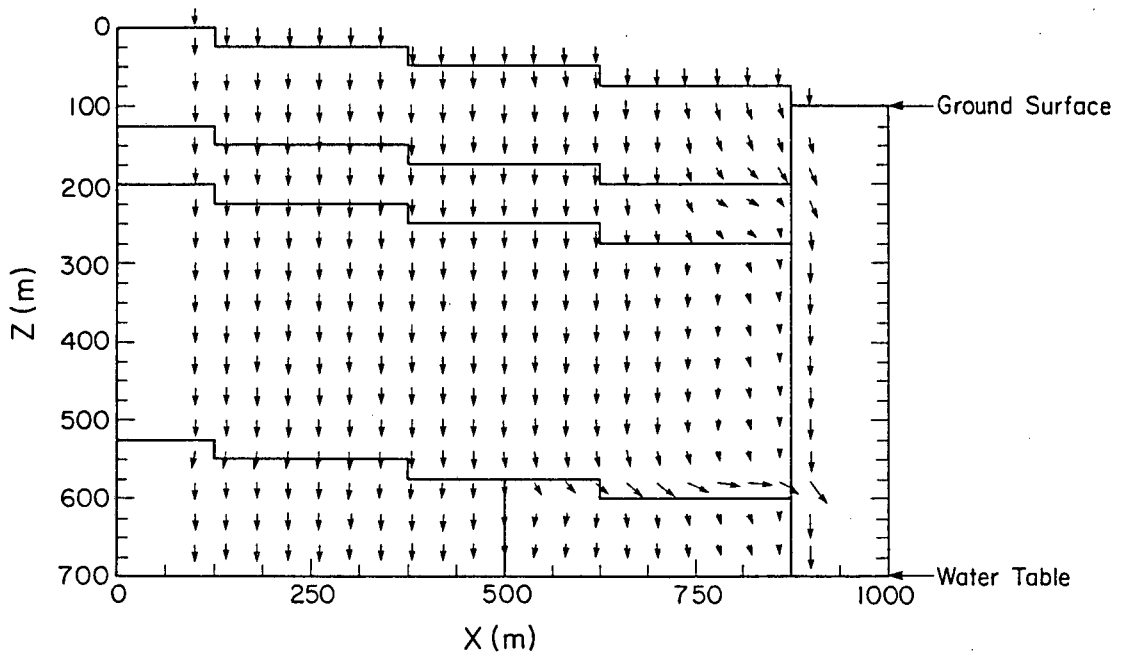

Infiltration Rate = 4.5 mm/yr

Figure 32. Vector plot of the computed mass flux through the flow system at steady state for Fracture-Matrix-Flow Simulation #2.

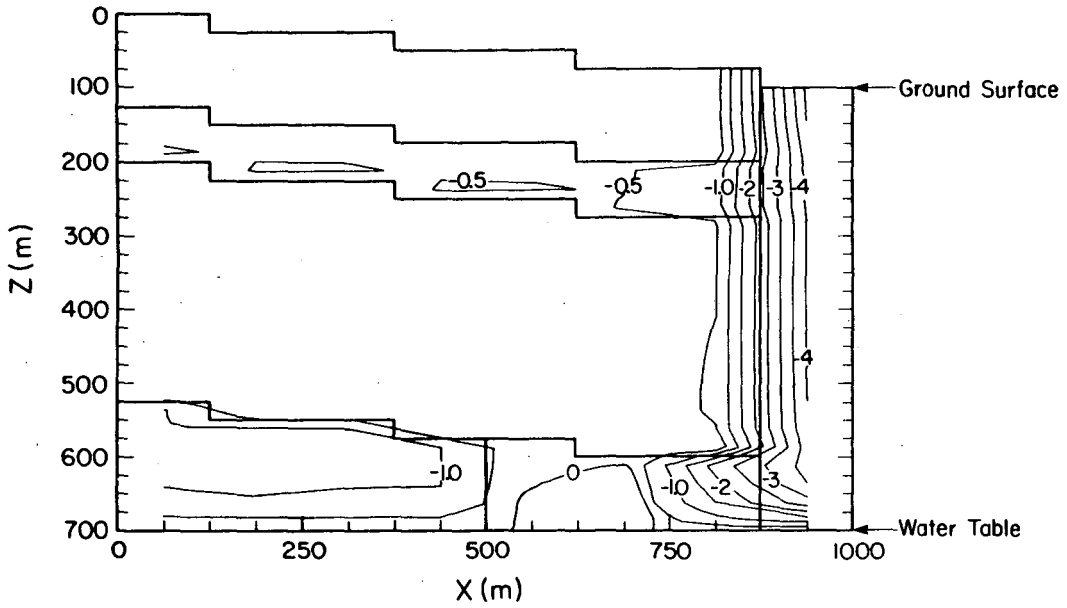

Infiltration Rate = 4.5 mm/yr
Contour Interval = 0.5 bar

XBL 856-10542

Figure 33. Contour diagram of the computed Matric-potential distribution at steady state for Fracture-Matrix Flow Simulation #2.

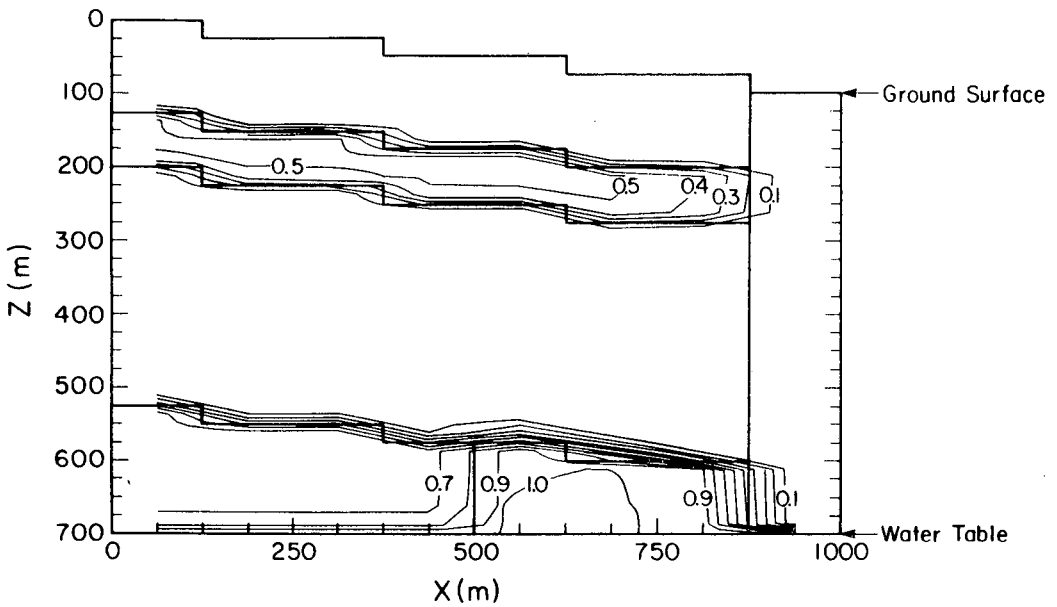

Infiltration Rate = 4.5 mm/yr
Contour Interval = 0.1

XBL 856-10544

Figure 34. Contour diagram of the computed liquid-saturation distribution at steady state for Fracture-Matrix Flow Simulation #2.

Fracture-Matrix Flow Simulation #1 in that, except where specified, the hydraulic properties of the units are identical to those used in FXMX1. In all cases, the infiltration rate is 4.5 mm/yr.

Fault-Zone Properties

The first sensitivity study was designed to examine the mass flux through the repository unit as a function of the absolute permeability of the Fault Zone and to investigate if perched water forms adjacent to the Fault Zone above the nonwelded units as the absolute permeability decreases. In all previous simulations, the Fault Zone was modeled as an anisotropic medium such that the vertical absolute permeability, $(k_a)_v$, was fifty times the horizontal absolute permeability, $(k_a)_h$. Therefore, to isolate the effect of changes in the absolute permeability, a run was performed in which the Fault Zone was modeled as an isotopic medium with $(k_a)_h=(k_a)_v=5x10^{-11}m^2$. Results of the simulations indicate that the steady-state solution is not sensitive to the change from anisotropic to isotropic conditions.

Four other simulations were performed. In one, k_a was increased; in the others, k_a was decreased. The results, summarized in Table 7, indicate that an increase in absolute permeability of 3 orders of magnitude from the base case ($k_a=5x10^{-11}m^2$) produces only a moderate decrease in the flux through the repository unit, from 3.5 mm/yr to 2.6 mm/yr. By reducing k_a 3 orders of magnitude, the flux through the repository unit increases from 3.5 mm/yr to 4.5 mm/yr. Lateral flow above the repository unit becomes insignificant, as evident in the vector plot of the mass flux, shown in Figure 35. Lateral flow into the Fault Zone occurs beneath the repository unit due to the relatively low permeability of the Calico Hills (zeolitic) nonwelded unit. There is a small component of flow from the Paintbrush nonwelded unit to the Fault Zone. There is also a small component of flow, obscured by the scale of Figure 35, from the Fault Zone into the welded units, except at the base of the Topopah Spring welded unit.

Table 7. Average computed flux through the repository unit as a function of the absolute permeability of the Fault Zone.

Absolute Permeability of Fault Zone (m^2)	Average flux through TSWU* (mm/yr)
5×10^{-8}	2.6
5×10^{-11} (base case)	3.5
5×10^{-12}	4.0
5×10^{-13}	4.2
5×10^{-14}	4.5

*TSWU = Topopah Spring Welded Unit

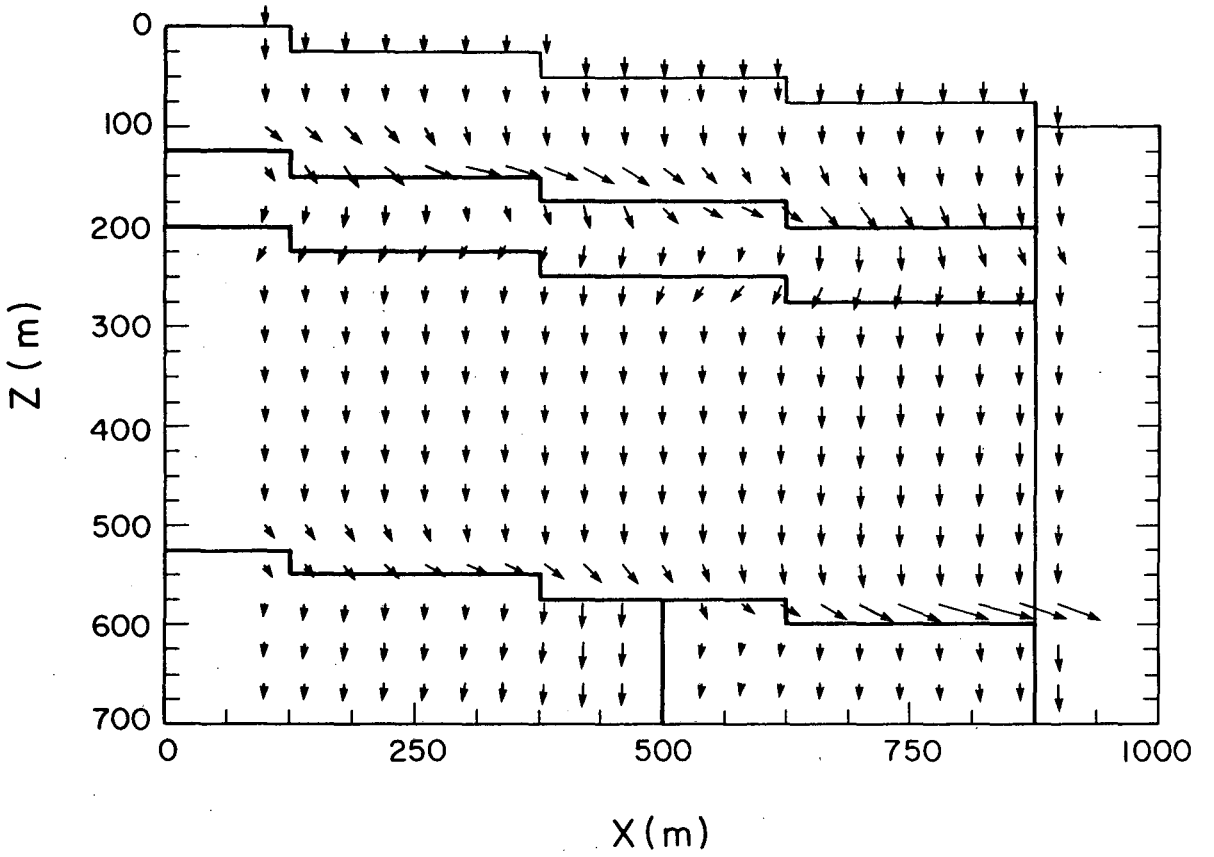

XBL 8510-12350

Figure 35. Vector plot of the computed mass flux through the flow system at steady state for the case in which the absolute permeability of the Fault Zone is reduced by three orders of magnitude.

Perched water formed within the top portion of the Calico Hills (zeolitic) nonwelded unit for the case in which the absolute permeability was 2 orders of magnitude less that the base case. For lower values of permeability, this zone of saturation extended to the water table and hence represents a rise in the water table rather than perched water.

Second Fault Zone

Another sensitivity study was designed to examine the effect of adding a second fault zone along the western boundary of the flow region, since Yucca Mountain is known to be bounded to the west by a steeply dipping, normal fault. The second fault zone, measuring 125 m by 700 m, was added onto the western edge of the flow region and was assigned the same hydraulic properties as the first one. All other aspects of the problem were identical to Fracture-Matrix Flow Simulation #1.

Figure 36 shows the vector plot of mass flux through the system at steady state. Lateral flow occurs at the base of the welded units and is directed into both fault zones. Above the repository unit, seven percent of the flow is diverted into the western fault zone and seventeen percent is diverted into the eastern fault zone. At the base of the repository unit, an additional one percent of the flow is diverted into the western fault zone and an additional twenty-one percent is diverted into the eastern fault zone. The average flux through the repository unit is 3.1 mm/yr.

The effect of adding a second fault zone is summarized in Table 8. Results indicate that the addition of a fault zone along the western boundary of Yucca Mountain decreases the flux through the repository unit due to additional lateral flow above the unit. However, the effects are rather small since the addition of a second fault reduced the average flux through the repository unit by only eleven percent.

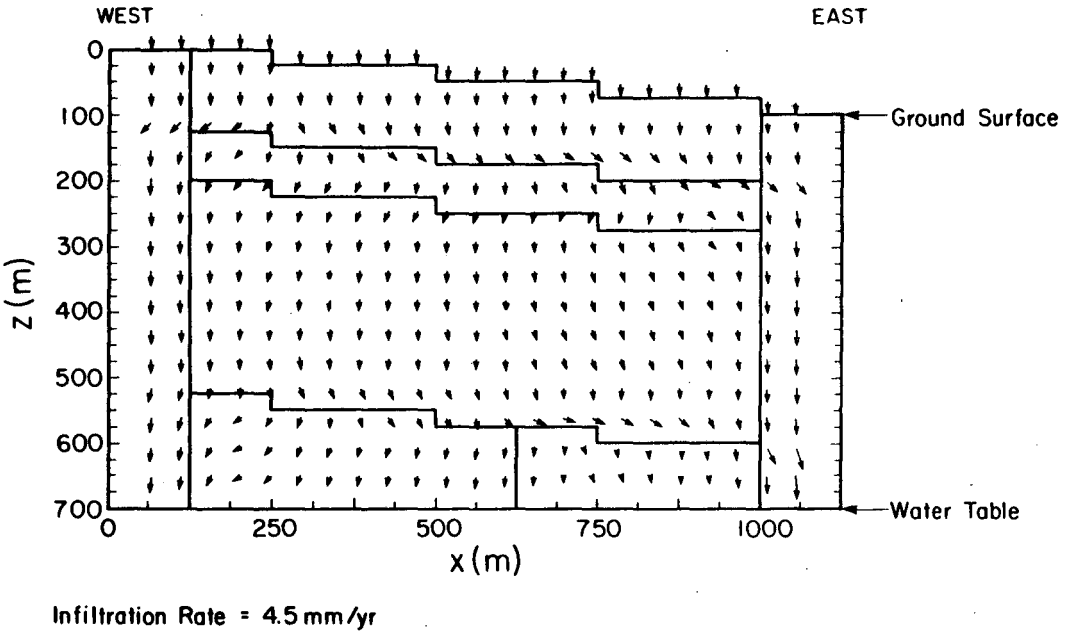

Figure 36. Vector plot of the computed mass flux through the flow system at steady state for the case of two fault zones.

Table 8. Summary of the effect of adding a second fault zone.

	One Fault Zone	Two Fault Zones
Percentage of computed flow diverted laterally into Fault Zone		
a) above TSWU*	20	24
b) below TSWU*	24	22
Average computed flux through TSWU* (mm/yr)	3.5	3.1

*TSWU = Topapah Spring Welded Unit

Mesh Dependence

In order to examine the effect of discretization errors, the sensitivity of the solution to the size of the elements was tested. The length of the elements was reduced from 125 m to 62.5 m. A repetition of Fracture-Matrix Flow Simulation #1 with this mesh indicated that the element size has a minor effect on the steady-state solution. The vector plot of mass flux was qualitatively unchanged; however, the average flux through the Topopah Spring welded unit increased slightly from 3.5 mm/yr to 3.7 mm/yr when the number of elements was doubled. Slight differences were observed in the contour diagrams of matric potential and liquid saturation; these are shown in Figures 37 and 38. The differences are not judged to be significant given the preliminary nature of this work and given the uncertainties regarding the material properties of the subsurface rocks at Yucca Mountain.

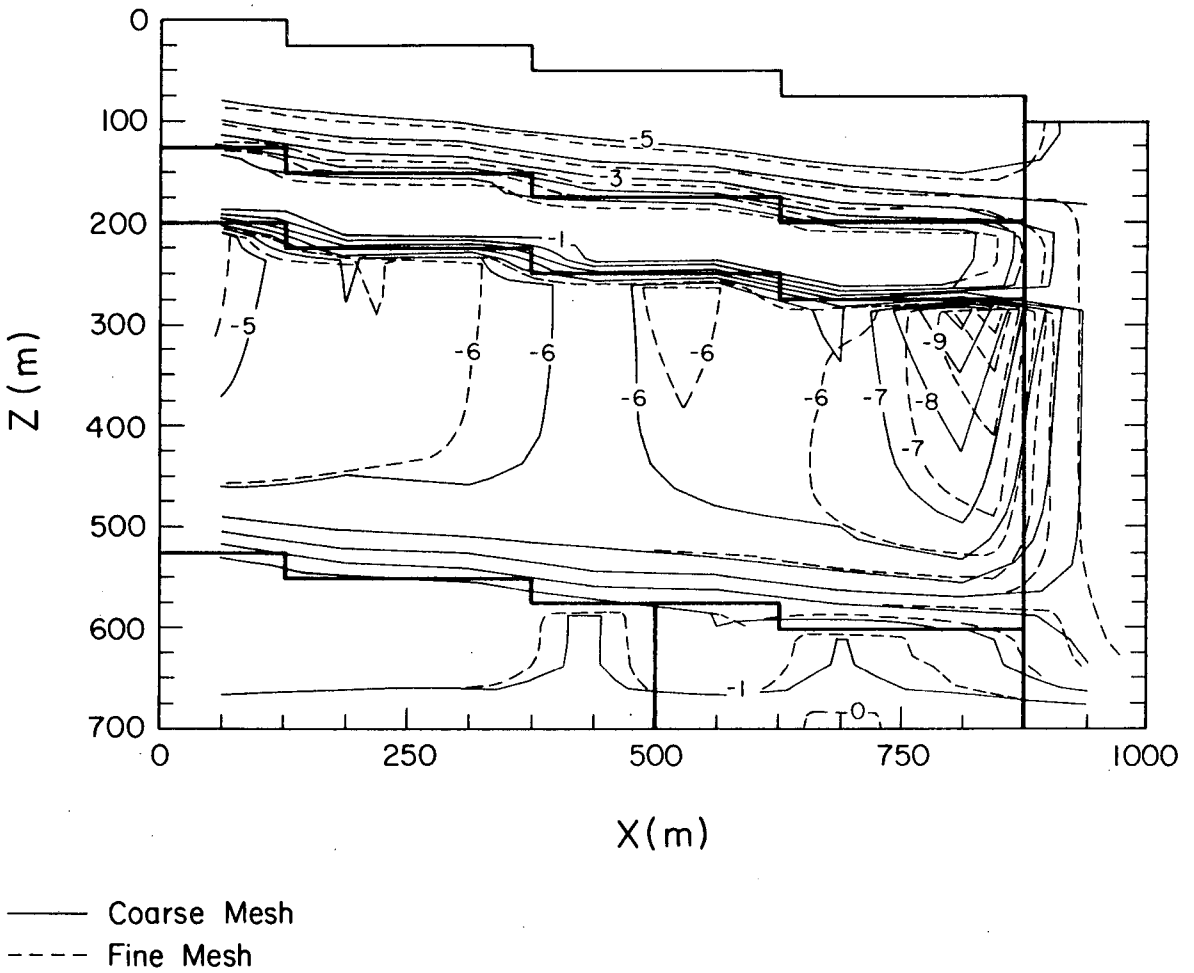

XBL 8510-12348

Figure 37. Contour diagram of the computed matric-potential distributions at steady state for a coarse mesh and a fine mesh.

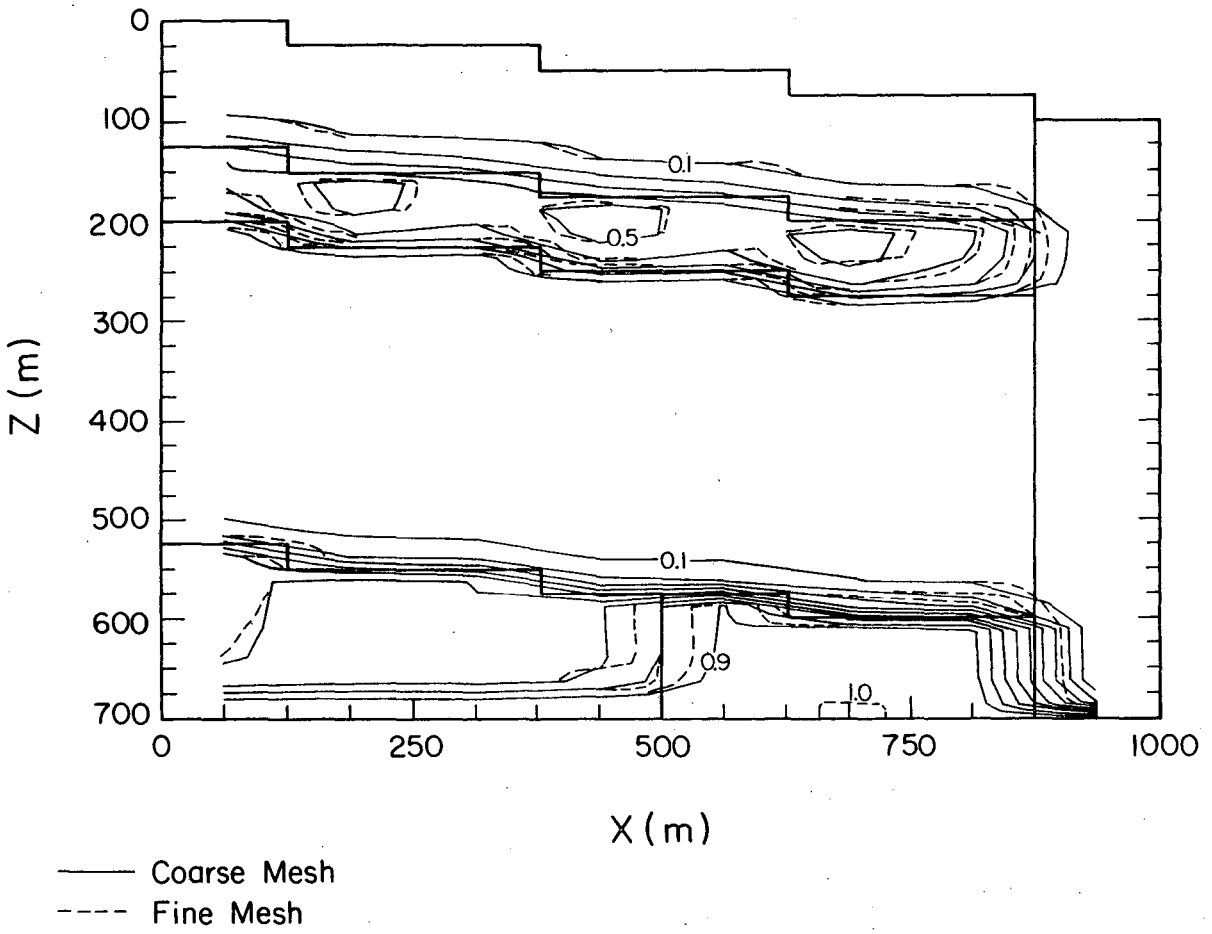

XBL 8510-12345

Figure 38. Contour diagram of the computed liquid-saturation distributions at steady state for a coarse mesh and a fine mesh.

6.0 DISCUSSION

In this section, results of the two-dimensional flow simulations are examined in terms of the available field data and the proposed conceptual model. To facilitate the discussion, the distinguishing features of the six, two-dimensional flow simulations are summarized in Table 9. The abbreviations listed in the second column are used for the remainder of the discussion.

6.1 Comparison with Field Data

The purpose of the following comparison is to identify and understand the causes of any major discrepancies between the simulation results and the field data. Two types of field data are available: (1) water potential versus depth from borehole USW UZ-1 (Figure 8), and (b) liquid saturation versus depth from borehole USW H1 (Figure 9). These are compared with the calculated values of matric potential and liquid saturation taken along the vertical section A-A' indicated in Figure 39. The location of A-A' coincides best with the location of borehole USW UZ-1. However, the lithology along A-A' is not identical to the lithology encountered in either borehole USW UZ-1 or USW H1. For example, in the simulations, the Tiva Canyon welded unit is 125 m thick, whereas at borehole USW UZ-1 this unit is absent, and at borehole USW H1 it is 10 m thick. The field data and simulation results cannot, therefore, be compared on the basis of depth alone; reference must be made to the appropriate lithologic column. Consideration must also be given to the sparseness and preliminary nature of the available data, and to the fact that the tuff units are modeled as homogeneous units when, in fact, they are not. Also, when reviewing the following discussion, one must bear in mind that the simulation results can never match both the liquid-saturation data and the matric-potential data for the repository unit because, as explained in Section 2.3.2, the field data are

Table 9. Distinguishing features of the six, two-dimensional flow simulations.

Simulation	Abbre-viation	Infiltration Rate (mm/yr)	Absolute Permeability of welded units	Type of characteristic curves used for TSWU*
Matrix-Flow #1	MX1	0.015	low	matrix (Figures 3b & 5b)
Matrix-Flow #2	MX2	1.0	low	matrix (Figures 3b & 5b)
Fracture-Flow #1	FX1	4.5	high	fracture (Figures 6a & 6b)
Fracture-Flow #2	FX2	1.0	high	fracture (Figures 6a & 6b),
Fracture-Matrix Flow #1	FXMX1	4.5	high	combined (Figures 6a & 29), AEV** = - 1.34
Fracture-Matrix Flow #2	FXMX2	4.5	high	combined (Figures 6a & 31), AEV** = - 0.0134

*TSWU = Topopah Spring welded unit / **AEV = Air-entry value in bars.

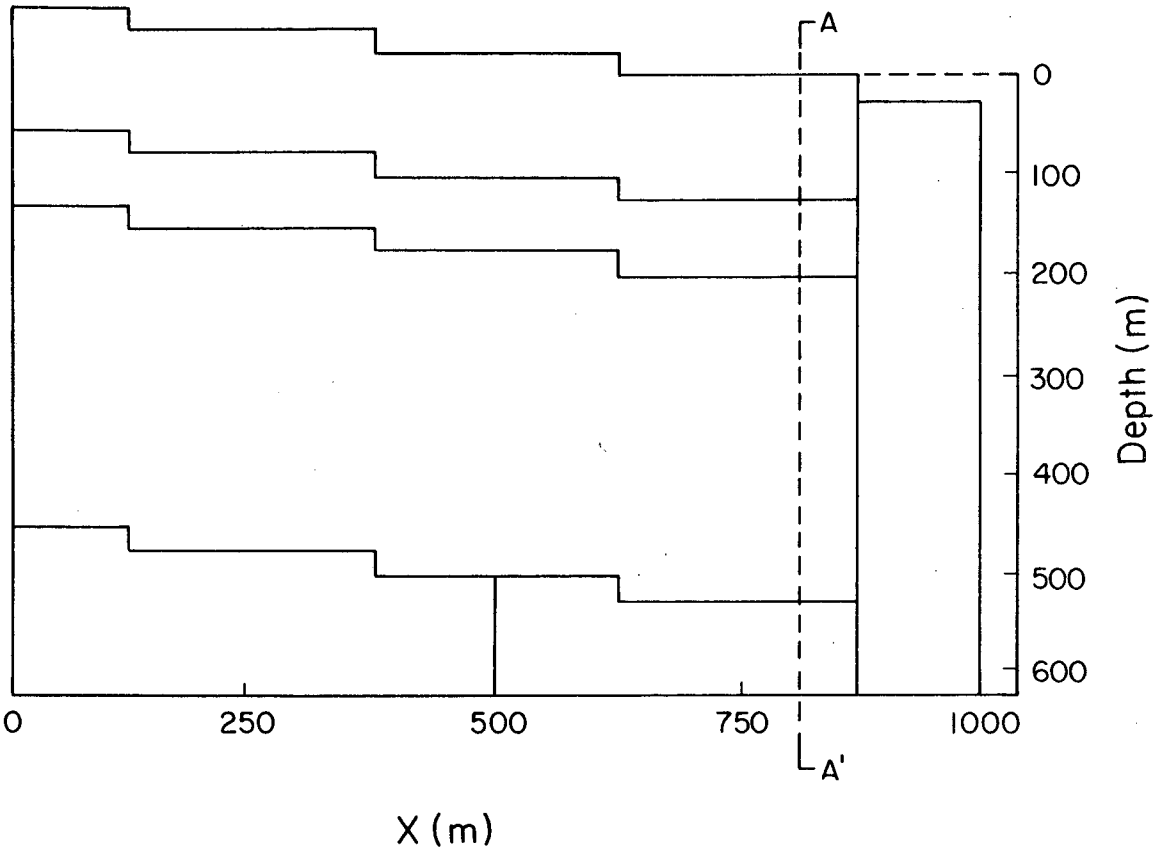

XBL 8510-12344

Figure 39. Location of vertical section A-A' corresponding to the location of borehole USW UZ-1.

inconsistent with the characteristic-curve data. In the present study, the comparison between field data and theoretical results is general and concentrates on the potential repository unit, the Topopah Spring welded unit.

6.1.1 Matric Potential

Figure 40 shows the profiles of matric potential along A-A' for each of the two-dimensional simulations. The in-situ data shown in Figure 8 indicate that the matric potential generaly increases with depth in the repository unit, and that the values range between -1 bar and -10 bars. In contrast, none of the simulations predicts a general decrease in matric potential with depth. In fact, three of the simulations, FX1, FX2, and FXMX1, predict an increase with depth due to the occurrence of lateral flow at the base of the repository unit. In FXMX2 and the matrix-flow simulations, flow beneath the Paintbrush nonwelded unit is generally one-dimensional and matric potential is nearly depth invariant.

All of the simulations except FX2 indicate that the matric potential is generally greater than -10 bars in the repository unit. FX2 is the case of fracture-matrix flow for a low infiltration rate of 1.0 mm/yr and an air-entry value of -1.34 bars. Of the remaining, MX1 provides the closest agreement with the observed data, with an average matric potential of approximately -3 bars. Recognize, however, that by changing the infiltration rate or by modifying the characteristic curves, the simulations could be manipulated to provide any desired average of value of matric potential in the repository unit.

6.1.2 Liquid Saturation

Computed profiles of liquid saturation are shown for the two-dimensional simulations in Figure 41. As explained in Section 5.2.2, the liquid saturation values in the Topopah Spring welded unit for the fracture- and fracture-matrix flow simulations have

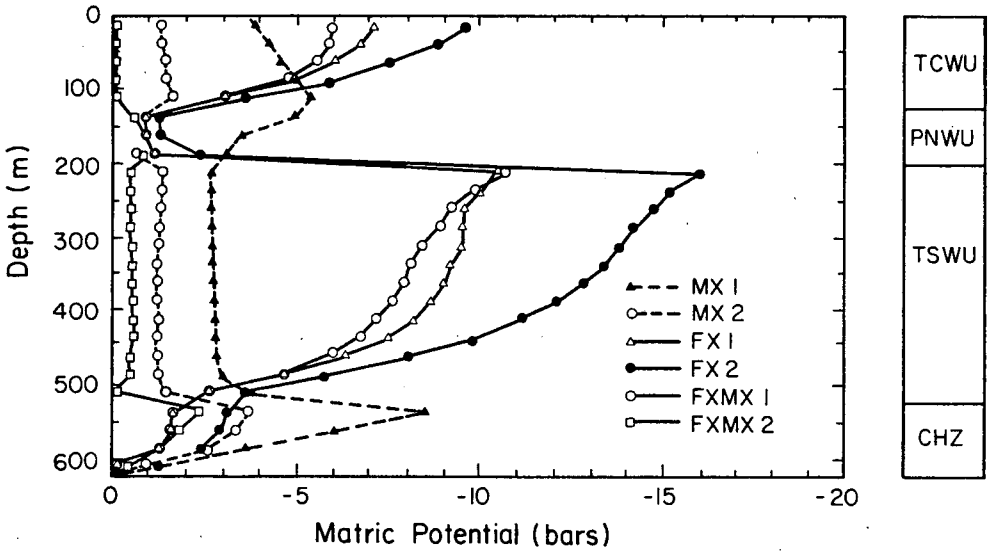

TCWU = Tiva Canyon Welded Unit
PNWU = Paintbrush Non Welded Unit
TSWU = Topopah Spring Welded Unit
CHZ = Calico Hills (zeolitic) Non Welded Unit

Figure 40. Comparison of the profiles of calculated matric potential along A-A' for the six 2-dimensional simulations.

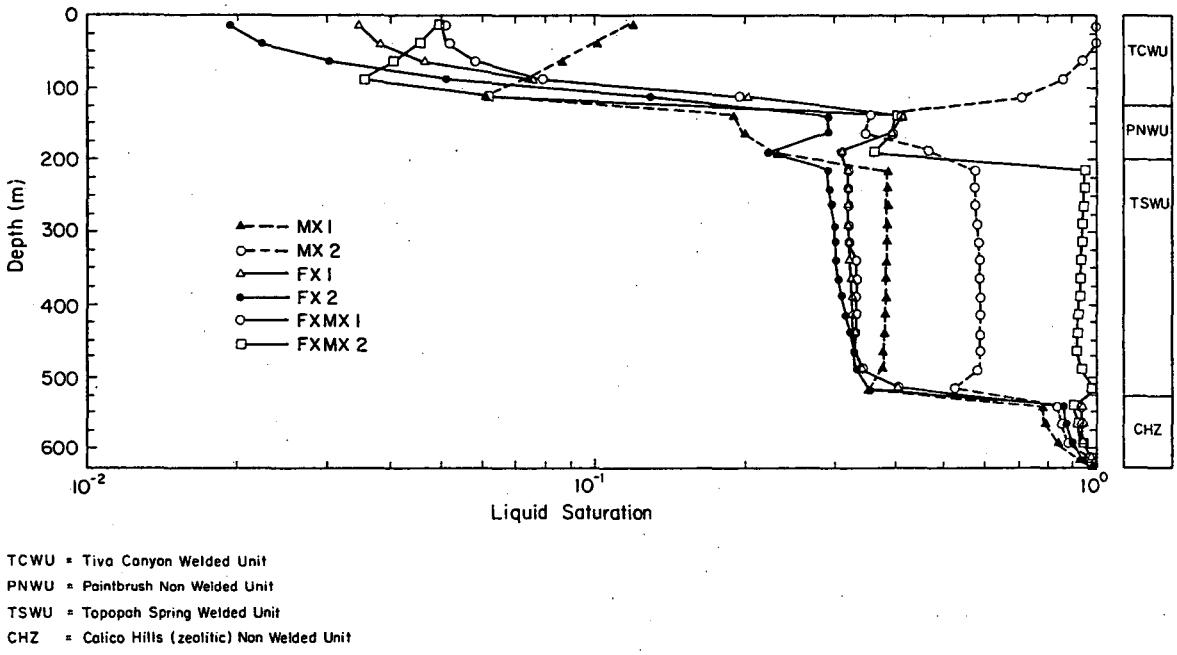

Figure 41. Comparison of the profiles of calculated saturation along A-A' for the six 2-dimensional simulations.

been obtained from the calculated steady-state value of matric potential and the moisture-retention curve shown in Figure 3b. The liquid saturations for the Topopah Spring welded unit therefore represent matrix saturations. Recall from Figure 9 that measurements made on samples of rock matrix generally increase in the repository unit from 0.30 to 0.80, and average approximately 0.65. From Figure 41 it is apparent that none of the simulations show a marked increase in liquid saturation with depth. However, MX2 predicts a uniform, average saturation of 0.6 and, therefore, provides the closest match with the observed liquid saturation profile.

With regard to the fracture- and fracture-matrix flow simulations, it is also of interest to note that the values of matrix saturation predicted by the simulations in which the air-entry value of the welded units was -1.34 bar (i.e. FX1, FX2, and FXMX1) are close to 0.30 whereas those predicted in the simulation using an air-entry value of -0.0134 bar are close to unity. The latter is consistent with the work of Wang and Narasimhan (1985) who show theoretically that steady-state fracture flow cannot occur until the matrix is nearly saturated.

6.2 Comparison with Conceptual Model

6.2.1 Matrix- Versus Fracture-Dominated Flow in Welded Units

To examine the effect of the assumption that flow in the welded unit units occurs in the matrix versus the fractures, MX2 and FX2 must be examined. Table 10 shows the salient features of the two runs. Less lateral flow occurs above the repository unit for fracture-flow conditions, although the difference is only nine percent. As a result, if all else is constant, the flux through the Topopah Spring welded unit is not particularly sensitive to the assumption of matrix- versus fracture-flow conditions, as modeled here. The results also show that lateral flow occurs at the base of the repository unit in FX2 and not in MX2 because the nonwelded units are less permeable than the welded units

Table 10. Comparison of the salient features of Matrix-Flow Simulation #2 and Fracture-Flow Simulation #2.

	Matrix-Flow Simulation #2	Fracture-Flow Simulation #2
Infiltration Rate (mm/yr)	1.0	1.0
Percentage of flow diverted laterally into Fault Zone a) above TSWU* b) below TSWU*	 48 0	 39 25
Average flux through TSWU* (mm/yr)	0.45	0.53
Range of matric potential in TSWU* (bars)	>-2	-4 to -16
Range of liquid saturation in TSWU*	0.5 to 0.95	0.29 to 0.35

*TSWU = Topopah Spring Welded Unit

when fracture-flow conditions are modeled. Lateral flow at the base of the repository unit has important implications with respect to the available flowpaths from the repository unit to the water table. For matrix-flow conditions, flowpaths are directed vertically from the Topopah Spring welded unit through the Calico Hills nonwelded unit to the water table. For fracture-flow conditions, there may be flowpaths directed from the Topopah Spring welded unit, along the top of the Calico Hills nonwelded unit, and then into the Fault Zone, where water is quickly transmitted to the water table. A detailed analysis of flowpaths and travel times have not been included in the study, however, due to the coarseness of the model and lack of data regarding the effective porosities of the units. Finally, the results listed in Table 10 indicate that if fracture-flow conditions are assumed, then the matric potential and liquid saturation are lower in the repository unit relative to the case in which matrix-flow conditions are assumed. This result is due entirely to the nature of the assumed characterisitic curves. One must bear in mind that the validity and generality of the conclusions from this comparison hinge on the validity of the, as yet, unverified theoretical fracture characteristic curves.

6.2.2 Lateral Flow

Lateral flow is an important feature of the conceptual model because it can reduce the amount of water that might otherwise travel through the repository. In the steady-state simulations, lateral flow is caused by permeability contrasts between adjacent units, anisotropy, and the dip of the layered units. Table 11 summarizes the information regarding lateral flow from the six, two-dimensional flow simulations. The results show that lateral flow can be significant, even for extremely low infiltration rates (eg., MX1). In the matrix-flow simulations, most of the lateral flow occurs within the Paintbrush nonwelded unit, whereas in the fracture- and fracture-matrix flow simulations, most of the lateral flow occurs within the welded units, just above the contact with the underlying nonwelded unit. A comparison of MX1 with MX2 or FX1 with FX2

Table 11. Comparison of the two-dimensional flow simulations in terms of lateral flow.

Simulation Name*	MX1	MX2	FX1	FX2	FXMX1	FXMX2
Net Infiltration Rate (mm/yr)	0.015	1.0	4.5	1.0	4.5	4.5
Percentage of flow diverted laterally into Fault Zone						
a) from Tiva Canyon welded unit	9	6	14	39	15	12
b) from Paintbrush nonwelded unit	48	42	5	0	5	1
c) from Topopah Spring welded unit	0	0	24	25	24	5
d) from Calico Hills nonwelded unit	0	0	0	0	0	0
Total	57	48	44	64	44	18
Average flux through Topopah Spring welded unit (mm/yr)	0.0053	0.45	3.5	0.53	3.5	3.8

*MX = matrix-flow; FX = fracture-flow; MXFX = combined, matrix-fracture flow

shows that for a given type of simulation, as the infiltration rate decreases, the amount of lateral flow above the Topopah Spring welded unit increases. This change is due to reduced permeabilities in the repository unit as the infiltration rate is reduced. The amount of lateral flow above the Topopah Spring welded unit is also a function of the absolute permeablitity of the Fault Zone. As demonstrated in Section 5.2.4, if the absolute permeability is decreased by three orders of magnitude, then lateral flow above the repository unit becomes negligible.

7.0 SUMMARY AND CONCLUSIONS

Yucca Mountain, located along the western edge of the Nevada Test Site, is a potential site for the construction of a mined geologic repository for storage of high-level radioactive waste. Evaluation of the site requires that the hydrogeologic system be understood so that reliable predictions of the transport of radionuclides from the repository to the accessible environment can be made. The hydrogeologic system at Yucca Mountain is extremely complex and, as yet, incompletely understood. The system is characterized by flow through heterogeneous, anisotropic, partially saturated, fractured tuff in an arid environment. As a first step toward understanding the system, Montazer and Wilson (1984) proposed a conceptual model based on their interpretation of the available data and the physics of flow through fractured media. In the present study, the numerical model TOUGH (Pruess, 1984) was used to examine the natural state of the unsaturated flow system at Yucca Mountain based on the available data and to test some of the hypotheses proposed by Montazer and Wilson (1984).

A series of steady-state numerical simulations were performed. The fractures at Yucca Mountain were incorporated into the analysis in an implicit fashion. The effects of the small scale tectonic fractures and cooling joints were incorporated into the characteristic curves of the highly fractured, welded units. The series of minor faults east of Yucca Mountain were modeled as a single, highly transmissive hydrogeologic unit. The simulations were of three general types: (1) the matrix-flow simulations, in which steady-state flow through the highly fractured welded units is assumed to occur solely within the rock matrix; (2) the fracture-flow simulations, in which steady-state flow through the welded units is assumed to occur solely within the fractures; and (3) the fracture-matrix flow simulations in which flow occurs through both the fractures and the matrix. For most types of simulations, the steady-state flow system was examined as a function of the infiltration rate. The results were expressed in terms of the magnitude and direction of mass flux through the system, the matric-potential distribution, and the

liquid-saturation distribution. Emphasis was placed on conditions in the potential repository unit, i.e., the Topopah Spring welded unit.

The conclusions from the study should be viewed as preliminary due to: (a) uncertainties in values used for the material properties of the units, (b) uncertainties in the estimates of net infiltration, and (c) the lack of field or laboratory experiments to verify that the numerical simulations produce results that are physically meaningful. Furthermore, extrapolation of the numerical results is inappropriate beyond the range of conditions investigated in this study due to the complex and nonlinear nature of the problem.

The conclusions are as follows:

1. In all of the two-dimensional flow simulations, lateral flow into the Fault Zone is an important feature of the modeled flow system, even for infiltration rates less than 1.0 mm/yr.
2. For a given type of simulation, a reduction in the infiltration rate leads to increased lateral flow above the Topopah Spring welded unit. For example, in the fracture-flow simulations, as the infiltration rate decreases from 4.5 mm/yr to 1.0 mm/yr, lateral flow above the Topopah Spring welded unit increases from twenty percent to forty percent of the available flow. This is due to the reduced permeability of the Topopah Spring welded unit for lower infiltration rates.
3. In the matrix-flow simulations, most of the lateral flow occurs within the Paintbrush nonwelded unit. In the fracture- and fracture-matrix flow simulations, most of the lateral flow occurs within the welded units, just above the contact with the underlying nonwelded unit. For example, under matrix-flow conditions, given an infiltration rate of 1.0 mm/yr, eighty-eight percent of the lateral flow occurs within the Paintbrush nonwelded unit, and twelve percent occurs within the Tiva Canyon welded unit. Under fracture-flow conditions, given the same infiltration rate, two percent of the lateral flow occurs within the Paintbrush nonwelded unit,

sixty-three percent occurs within the Tiva Canyon welded unit, and thirty-five percent occurs within the Topopah Spring welded unit. Flow through the Calico Hill nonwelded unit is dominantly vertical in all simulations.

4. If fracture-flow conditions dominate in the welded units, then lateral flow occurs at the base of the Topopah Spring welded unit. This condition has important implications with regard to available pathways for solute transport from the potential repository horizon to the water table. Specifically, if lateral flow occurs at the base of the Topopah Spring welded unit, then flowpaths may be directed around the Calico Hills nonwelded unit and into the Fault Zone where water is quickly transmitted to the water table.

5. For the conditions tested here, the flux through the Topopah Spring welded unit is increased only slightly if fracture-flow conditions are assumed as opposed to matrix-flow conditions. For an infiltration rate of 1.0 mm/yr, the average flux through the repository unit is 0.53 mm/yr for fracture-flow conditions and is 0.45 mm/yr for matrix-flow conditions.

6. By assuming fracture-flow conditions rather that marix-flow conditions, lower values are obtained for matric potential and liquid saturation in the repository unit. This is due entirely to the nature of the characteristic curves assumed in Matrix-Flow Simulation #2 and Fracture-Flow Simulation #2.

7. A reduction of the air-entry value assumed for the theoretical fracture characteristic curves from -1.34 bars to -0.0134 bar results in dominantly vertical flowpaths driven by the gravity-potential gradient. For the simulation conditions examined in the present study, lateral flow into the Fault Zone above the Topopah Spring welded unit was reduced by seven percent; lateral flow at the base of the Topopah Spring welded unit was reduced by nineteen percent.

8. The numerical simulations will never yield a match with both the observed liquid-saturation data and matric-potential data in the Topopah Spring welded unit. The

reason is that the characteristic curves show increasing matric potential with increasing liquid saturation whereas the field data suggest decreasing matric potential with increasing liquid-saturation with depth in the Topopah Spring welded unit. This discrepancy may be due to heterogeneity within the Topopah Spring welded unit as the measured values of matric potential and liquid saturation are extremely sensitive to variations in bulk density and changes in pore-size distribution.

9. With one exception, all the simulations indicate that the matric potential is generally greater than -10 bars in the repository unit, and are, therefore, in the same range as the in-situ data. The exception occurs for the fracture-flow simulation in which the infiltration rate is specified as 1.0 mm/yr; in this case, the matric potential varies from -4 to -16 bars. None of the simulations predicts a general decrease in matric potential with depth in the repository unit, as observed in USW UZ-1. In fact, the simulations that produce lateral flow at the base of the unit indicate a general increase in matric potential with depth. The matrix-flow simulations predict a depth-invariant profile.

10. The matrix-flow simulation with an infiltration rate of 1.0 mm/yr provides the best agreement between simulated profiles of liquid-saturation and data from borehole USW H1. The simulation predicts a depth-invariant liquid-saturation profile in the repository unit with an average value of 0.60 while the data indicate a general increase with depth from 0.30 to 0.80 with an average of 0.65. None of the simulations show a marked increase in liquid saturation with depth in the Topopah Spring welded unit.

11. In comparing simulation results and field data, consideration should be given to the sparseness and preliminary nature of the available data, and to the fact that the tuff units are modeled as homogeneous units when, in fact, they are not. In addition, by changing the infiltration rate and/or by modifying the characteristic

curves, the simulations can be manipulated to provide any desired average value of matric potential or liquid saturation in the repository unit. This type of calibration exercise is not appropriate at present in view of the sparse data set and the uncertainty in knowledge of the material properties and flow mechanisms.

12. The average flux through the repository unit is moderately sensitive to the absolute permeability of the Fault Zone, assuming fracture-matrix flow conditions and an infiltration rate of 4.5 mm/yr. By reducing the absolute permeability by three orders of magnitude from the base value of 5×10^{-11} m^2, the average flux increases from 3.5 mm/yr to 4.5 mm/yr and the net lateral flow above the Topopah Spring welded unit is zero.

13. Perched water forms within the top portion of the Calico Hills (zeolitic) nonwelded unit for the case in which the absolute permeability of the Fault Zone is reduced by two orders of magnitude from the base value. For lower values of permeability, this zone of saturation extended to the water table and hence represents a rise in the water table rather than perched water.

14. The flux through the repository unit is only weakly sensitive to the addition of a second fault zone along the western boundary of the flow region. For an infiltration rate of 4.5 mm/yr and for fracture-flow conditions, the addition of a second fault zone reduced the average flux through the repository unit from 3.5 mm/yr to 3.1 mm/yr.

15. A reduction of the length of the elements by a factor of two produced only a minor effect on the steady-state solution. The slight differences were not judged to be significant given the preliminary nature of this study and given the uncertainties regarding the material properties and flow mechanisms.

Much additional work is needed before reliable models of the natural state of the Yucca Mountain system can be developed. Specifically, the following activities would be helpful:

1. Laboratory and field experimentation is needed to determine the conditions that lead to matrix flow in the unsaturated tuff and the conditions that lead to fracture flow.
2. Reliable measurements of the net infiltration to the system are needed. This information is critical for predictions of the amount of lateral flow above the repository unit, and hence, predictions of the average flux through the repository horizon, as well as for travel time calculations.
3. In-situ measurements of the material properties are needed, especially with regard to the absolute permeability of the units.
4. Reliable measurements of the effective matrix porosity and fracture porosity of the units are needed. These are required in the travel-time calculations and may vary over several orders of magnitude, depending upon whether fracture or matrix porosities are considered.

Future numerical work might include:

1. Removal of the restriction of homogeneity and incorporation of the spatial variability of the material properties, as data permit;
2. Incorporation of the flow of heat and air.
3. Incorporation of major structural features, such as shear zones and faults that may form conduits for water flow;
4. Investigation of the sensitivity of the solutions to the choice of characteristic curves;
5. Investigation of the importance of hysteresis and the transient formation of capillary barriers.

6. Use of a more realistic representation of the boundary between the zeolitic and vitric facies of the Calico Hills nonwelded unit. In the present study, the boundary was vertical; a horizontal boundary may be more appropriate.

7. Extend the simulations to consider the three-dimensional nature of the groundwater flow system.

And, finally, the theoretical study presented in this report suggest that the following types of data should be included in future data-collection programs:

1. More in-situ profiles of matric potential and liquid saturation are needed. Preferably, these data should come from the same borehole to provide in-situ moisture-retention data.

2. Measurements of relative-permeability curves for the matrix of consolidated rock are needed. In this report, methods were used that were developed for unconsolidated soils to predict the relative-permeabilty curve, given moisture-retention data. The applicability of this method to consolidated rock will remain at issue until measurements are available for validation. These measurements are especially important since the relative-permeability curve controls much of the behavior of the flow system.

3. Measurements of both the moisture-retention curve and the relative-permeabilty curve are needed for fractured rock. With these data, the validity of the theoretically derived fracture characteristic curve could be tested.

4. Features that may form a conduit for flow from the repository horizon to the Fault Zone, where travel times to the water table are short, need to be identified.

References

Bodvarsson, G. S., and J. J. Rulon, Studies of liquid infiltration in unsaturated fractured rock, Earth Sciences Division Annual Report 1985, Lawrence Berkeley Laboratory, in press, 1985.

Brooks, R. H. and A. T. Corey, Hydraulic properties of porous media, Hydrology Paper No. 3, Colorado State University, Ft. Collins, Colorado, 1964.

Carr, W. J., Byers, F. M., Jr. and P. P. Orkild, Stratigraphic and volcano-tectonic relations of Crater Flat Tuff and some older volcanic units, Nye County, Nevada: U.S. Geological Survey Open-File Report 84-114, 42 pp., 1984.

Duff, I. S., MA28 - A set of FORTRAN subroutines for sparse unsymmetric linear equations, AERE Harwell Report R8730, July, 1977.

Edwards, A. L., TRUMP: A computer program for transient and steady-state temperature distributions in multi-dimensional system, National Tech. Info. Ser., UCRL 14754, Rev. II, Springfield, Virginia, 22151, 265 pp., 1969.

Herkelrath, W. N. and C. F. O'Neal II, Water vapor adsorption in low-permeability rocks, Proceedings of 17th International Congress, International Association of Hydrogeologists, January 7-12, Tuscon, Arizona, 1985.

Hillel, D., Applications of Soil Physics, Academic Press, New York, 385 pp., 1980.

International Formulation Committee, A formulation of the thermodynamic properties of ordinary water substance, IFC Secretariat, Dusseldorf, Germany, 1967.

Millington, R. J. and J. P. Quirk, Permeability of porous solids, Trans. Faraday Soc., Vol. 57, pp. 1200-1206, 1961.

Montazer, P. and P. E. Harrold, A theoretical model for fluid flow in unsaturated fractured media, in preparation, 1985.

Montazer, P. and W. E. Wilson, Conceptual hydrologic model of flow in the unsaturated zone, Yucca Mountain, Nevada: U.S. Geological Survey Water Resources Investigations Report 84-4345, 55 pp., 1984.

Montazer, P., Hammermeister, D. P. and M. S. Whitfield, Drilling, Instrumentation and preliminary testing results of borehole USW UZ-1 penetrating thick unsaturated tuffs, Yucca Mountain, Nye County, Nevada, Water Resources Investigation series in preparation, 1985.

Narasimhan, T. N. and Witherspoon, P. A., An integrated finite difference method for analyzing fluid flow in porous media, Water Resources Research, Vol. 12, No. 1, pp. 57-64, 1976.

Peters, R. R., Klavetter, E. A., Hall, I. J., Blair, S. C., Hellers, P. R. and G. W. Gee, Fracture and matrix hydrologic characteristics of tuffaceous materials from Yucca Mountain, Nye County, Nevada, Sandia Report SAND84-1471, December 1984.

Pruess, K., TOUGH: A numerical model for strongly driven heat flow in partially saturated media, Annual Report of the Earth Sciences Division, Lawrence Berkeley Laboratories, 1983.

Quiring, R. F., Precipitation climatology of the Nevada Test Site: National Oceanic and Atmospheric Administration, National Weather Service Report WSNSO 351-88, 34 pp., 1983.

Robison, J. H., Ground-water level data and preliminary potentiometric-surface maps of Yucca Mountain and vicinity, Nye County, Nevada: U.S. Geological Survey Water-Resources Investigations Report 84-4197, 8 pp., 1984.

Scott, R. B. and J. Bonk, Preliminary geologic map of Yucca Mountain with geologic sections, Nye county, Nevada: U.S. Geological Survey Open-File Report 84-494, scale 1:12,000, 1984.

Scott, R. B., Spengler, R. W., Diehl, S., Lappin, A. R. and and M. P. Chornack, Geological character of tuffs in the unsaturated zone at Yucca Mountain, Southern Nevada, in Mercer, J. W. Rao, P.S.C. and I. W. Marine, eds., Role of the Unsaturated Zone in Radioactive and Hazardous Waste Disposal; Ann Arbor, Michigan, Ann Arbor Science, pp. 289-335, 1983.

van Genuchten, M. T., A closed-form equation for predicting the hydraulic conductivity of unsaturated soils, Soil Sci. Soc. Am. Jour., Vol. 44, pp. 892-898, 1980.

Waddell, R. K., Robison, J. H. and R. K. Blankennagel, Hydrology of Yucca Mountain and vicinity, Nevada-California--Investigative results through mid-1983, U.S. Geological Survey Water Resources Investigations Report 84-4267, 72 pp., 1984.

Wang, J. S. Y. and T. N. Narasimhan, Hydrologic mechanisms governing fluid flow in partially saturated, fractured porous medium, in press, Water Resources Research, 1985.

Weeks, E. P. and W. E. Wilson, Preliminary evaluation of hydrologic properties of cores of unsaturated tuff, test well USW H-1, Yucca Mountain, Nevada: U.S. Geological Survey Water Resources Investigations Report 84-4193, 30 pp., 1984.

Winograd, I. J. and Thordarson, W., Hydrogeologic and hydrochemical framework, south-central Great Basin, Nevada-California, with special reference to the Nevada Test Site: U.S. Geological Survey Professional Paper 712-C, 126 pp., 1975.

This report was done with support from the Department of Energy. Any conclusions or opinions expressed in this report represent solely those of the author(s) and not necessarily those of The Regents of the University of California, the Lawrence Berkeley Laboratory or the Department of Energy.

Reference to a company or product name does not imply approval or recommendation of the product by the University of California or the U.S. Department of Energy to the exclusion of others that may be suitable.

LAWRENCE BERKELEY LABORATORY
TECHNICAL INFORMATION DEPARTMENT
UNIVERSITY OF CALIFORNIA
BERKELEY, CALIFORNIA 94720